INTERNAL POLARIZATION EFFECT IN PEROVSKITE SOLAR CELLS

by

Fangda Yu

B.S, University of Pittsburgh, 2014

B.S, Beihang University, 2014

Submitted to the Graduate Faculty of

Swanson School of Engineering in partial fulfillment

of the requirements for the degree of

Master of Science

University of Pittsburgh

2015

UNIVERSITY OF PITTSBURGH

SWANSON SCHOOL OF ENGINEERING

This thesis was presented

by

Fangda Yu

It was defended on

November 20th, 2015

and approved by

Jung-Kun Lee, PhD, Associate Professor

Department of Mechanical Engineering and Materials Science

Qing-Ming Wang, PhD, Professor

Department of Mechanical Engineering and Materials Science

Ian Nettleship, PhD, Associate Professor

Department of Mechanical Engineering and Materials Science

Thesis Advisor: Jung-Kun Lee, PhD, Associate Professor

INTERNAL POLARIZATION EFFECT IN PEROVSKITE SOLAR CELLS

Fangda Yu, M.S.

University of Pittsburgh, 2015

Rapid development of perovskite solar cells (PSCs) in recent years has attracted a lot of attention in the photovoltaic research field. Two types of TiO_2 nano-scaled morphologies, nanoparticle and nanowire, play an important role in PSCs as a scaffold for the photoactive component of the PSCs. These two different morphologies also result in different electron transporting behavior in PSC. In this thesis, PSC samples are fabricated using both types of morphologies and their photovoltaic behaviors are compared with each other. Single crystalline rutile TiO_2 nanowire is fabricated on fluorine doped tin oxide (FTO) substrates by a microwave assisted hydrothermal method. This method is very sensitive to many parameters, which cause TiO_2 nanowire samples with multiple lengths, densities and aspect ratios to be fabricated. TiO_2 nanoparticle layer is fabricated by spin coating TiO_2 mesoporous paste on an FTO substrate. The TiO_2 nanowire based PSC has a power convert efficiency (PCE) of 14.5% and TiO_2 nanoparticle based PSC's has a PCE of 12.9%. Photovoltaic measurements are applied to explain the carrier transport behavior. I-V measurement shows that the hysteresis effect in TiO_2 nanoparticle based PSC is large. IPCE measurement shows that the illumination frequency dependence of photocurrent in

TiO_2 nanowire based PSC is large. As the illumination frequency increases, the photocurrent of PSCs at the short circuit condition decreases. Electron lifetime measurement presents the electron diffusivity and lifetime are longer in the nanowire based PSCs. Space charge polarization phenomenon is introduced to explain the different photovoltaic performance of the nanowire and nanoparticle based PSCs.

TABLE OF CONTENTS

LIST OF TABLES

LIST OF FIGURES

NOMENCLATURE

EHP	Electron-hole pair
FTO	Fluorine doped tin oxide
ITO	Indium doped tin oxide
TCO	Transparent conducting oxide
PSC	Perovskite solar cell
DSSC	Dye-sensitized solar cell
VB	Valence band
CB	Conduction band
E_F	Fermi energy level
DC	Direct current
AC	Alternate current
PCE	Power covert efficiency
IPCE	Incident photon-to-current efficiency
I_{sc}	Short-circuit current
J_{sc}	Short-circuit current density
V_{oc}	Open-circuit voltage
FF	Fill factor
UV/Vis	Ultraviolet-visible spectroscopy

h	Planck constant
τ_e	Electron lifetime
τ_{tr}	Transport time coefficient
I_S	Saturation current
χ	Volume ratio
σ	Conductivity
ρ	Resistivity
NW	Nanowire
NP	Nanoparticle
%T	Transmittance
A	Absorbance
%R	Reflectance
λ	Wavelength
Δn_p	Excess electron concentration
n_p	Total electron concentration
G_{ph}	Photogeneration rate
g(E)	Dense of state
E_c	Energy of conduction band
E_v	Energy of valance band
D	Diffusivity
τ_c	Exponential decay time constant
τ_n	Electron lifetime

ACKNOWLEDGMENT

I would have great and sincere thanks to my advisor, Prof. Jung-Kun Lee for his patience, generousness and considerable help throughout my study and research. Without his guidance and support, I would have never accomplished my research.

I would also thank my committee members: Prof. Qing-Ming Wang, Prof. Ian Nettleship and Dr. Jung-Kun Lee for their time to make this thesis better.

I have my thanks to my excellent upper class students in my research group: Dr. Gill-Sang Han, Po-Shun Huang, Salim Caliskan and Ziye Xiong for sharing priceless experience on experiments. My thanks also go to my lab partners: Jinsun Yoo, Matthew Lawrence Duff, Yenjung Tu and Seongha Lee for their kind help.

Finally, I would thanks to my family for supports and encouragements.

1.0 INTRODUCTION

Titanium oxide, also named as titania, has a chemical formula of TiO_2. It is an outstanding material with high stability, refractive index. It can be found in natural ores and used as a pigment. Nowadays, it can also be used as photocatalysts, photovoltaics and sensors for its unique electric and optical properties. Recently, the application of TiO_2 nanostructures in solar cells has been widely used, including dye-sensitized solar cell (DSSC) and perovskite solar cell because TiO_2 has high conductivity and transparency, which means only low number of photons loss during their incidence. However, TiO_2 does have problems exist, such as large band gap, which causes insufficient utilize of solar energy, and slow carrier transport, which increases carrier recombination possibility.

TiO_2 has three crystal structures that can be found in nature: rutile, anatase and brookite, where rutile and anatase are a tetragonal structure while brookite is an orthorhombic structure. Rutile is the most abundant structure among these three phases in the nature. The ratio of the rutile phase in the natural ore is 98%. Anatase and brookite are metastable phase of TiO_2 and convert to a stable phase rutile at 600 to 800℃. [45]

The perovskite solar cell using the organic-inorganic compound has become an important topic for solar cell research field these years, since its fabrication steps are simpler and cheaper compared with traditional silicon solar cell. The traditional silicon solar cells, however, require a complicated process, a long production cycle and consumes large energy. The processing steps

include purifying the silicon, where the single crystal Si with at least 99% purity is produced from silicon dioxide, such as quartz. Usually the purification occurs at temperature up to 1000°C, and vacuums in special clean room facilities in order to achieve the high purity. [1] Most attractively, people has created methylammonium lead trihalides, which has a perovskite structure, using various solvent techniques, such as one step and two step method, of which have the high potential to move on. [3] During solution processing, lead halide and methylammonium iodide can be dissolved in solvent and spin coated on a substrate, which is economically viable and suitable for mass production. Solvent evaporation and solute sediment during spin-coating results in dense layers of well crystallized perovskite material. Though simple solution processing results in the presence of voids, and other defects in the layer, which would decrease the efficiency of a solar cell, however, another technique using room temperature solvent to solvent extraction produces high-quality crystalline films. In vapor based techniques, spin coated lead halide is annealed in the presence of methylammonium iodide vapor at a temperature around 150 °C. [4] This method have an advantage that it gives the possibility for multi-stacked thin films over larger areas and this could be useful for producing multi-junction cells. In addition, vapor deposited techniques result in less thickness variation than simple solution processed layers.

Rutile TiO_2 is the most commonly used material in perovskite solar cell as the scaffold. The overall conductivity of light absorber layer in perovskite solar cell is increased due to its presence. Nanowire and nanoparticle are the two nanostructure of TiO_2 that have been mostly studied. Both of these nanostructures can produce perovskite solar cell with good properties. However, the carrier transporting behaviors in these structures are still a topic in research field. In nanoparticle structure, some people believe the electrons go through the TiO_2 nanoparticle

while other believe the electrons only transport through perovskite grains, which means the presence of TiO_2 nanoparticle did nothing to the carrier transportation. For nanowire structure, previous results showed that electron diffusion coefficient is larger in nanowire structure than that in nanoparticle structure in DSSC. [21]

In this thesis, the behavior of carrier transporting and internal polarization effect in rutile TiO_2 nanowire based perovskite solar cell will be studied. TiO_2 nanowires were grown on dense TiO_2 coated FTO substrate by using microwave assisted hydrothermal method. In order to get ideal TiO_2 nanowire features, with different length, density and aspect ratio, different nanowire growth solutions were used. SEM images were taken for checking TiO_2 nanowire substrates' features. Perovskite solar cells (PSC), including reference TiO_2 nanoparticle based PSC and TiO_2 nanowire based PSC, were fabricated through a series of fabrication steps involving spin coating and water phase treatment. In order to test how many photons are absorbed by perovskite solar cell samples, transmittance, absorbance and reflectance of perovskite solar cell samples were measured as a function of the wavelength of incident photon by ultraviolet-visible spectroscopy. Static photovoltaic measurements, including I-V curve measurement and DC mode incident photon-to-current efficiency, and dynamic photovoltaic measurement including AC mode incident photon-to-current efficiency and carrier lifetime measurement, are used to study the carrier transportation behavior.

This thesis is organized in chapters as follows. Brief introduction on TiO_2 and perovskite solar cell is introduced in chapter 1. Chapter 2 discusses the background information of semiconductor and solar cell. Basic concepts like Fermi-energy level, p-n junction and carrier recombination are included. A literature review on perovskite solar cell is also included in this chapter. Chapter 3 is containing hypothesis and objective of this thesis. The tasks for achieving

the objective are also contained in chapter 3. Chapter 4 presents the experimental details. Different condition of nanowire growth solutions, fabrication steps of perovskite solar cells and operation detail of measurements are given. Chapter 5 is for showing the data and result from the experiment. SEM images of TiO_2 nanowire substrates describe the features of the sample. Photovoltaic measurements showed the property of perovskite solar cell. Chapter 6 is the overall conclusions and future works of this thesis.

2.0 BACKGROUND INFORMATION AND LITERATURE REVIEW

This chapter is mainly introducing some common knowledge of semiconductor, P-N junction and solar cells. Basic concepts and behaviors such as Fermi-Energy level, space charge polarization and carrier recombination will be introduced. In order to have a better understanding on perovskite solar cell, which is the core of this thesis, a brief introduction will also be included in this chapter.

2.1 SEMICONDUCTOR

Semiconductor is a type of material, which exhibits electric conductivity in between of conductor such as metal, and insulator such as rubber. Unlike metals where electrons only stay on conduction band, in semiconductor, electrons stay in valence band. When the lattice is treated with thermal or photo excitation, the electrons are excited into conduction band and leave a hole in its previous site. This electron and its corresponding hole are called electron-hole pair (EHP). Thus, semiconductor becomes conductive due to the motion of EHP.

There are two general types of semiconductor. One type is formed by elemental substance, like silicon and germanium, which can be found in the group IV on the periodic table. The second type, on the other hand, is formed by chemical compound, especially by group IIIA and group VA, such as GaAs. [2] Recently transparent conducting oxide (TCO), which is also a

type of semiconductor, has attracted considerable attention for its low resistivity and high transparency. Some products like fluorine doped tin oxide (FTO) and indium doped tin oxide (ITO) have already been widely used in photovoltaics and displays. Other TCO like zinc oxide and titanium oxide also play an important role in this field.

One significant difference between conductor and semiconductor is their band structure. In conductors like metals, electron energy levels are continuously distributed. However, a band gap exists between conduction band and valence band in semiconductor. The reason is in metals, the wave vectors of Brillouin zone boundaries in different crystal directions, such as [100], [110] and [111] can overlap with each other to form a continuous shape. However, in semiconductors, though wave factors in different directions can overlap each other, they cannot form a continuous shape. Thus, semiconductors have a band gap. [20]

In order to determine the number of free electrons and free holes the conduction band and valence band of the semiconductor, the density of quantum state needs to be calculated.

$$g(E) = ((8\sqrt{2}\pi)\left(\frac{m}{h^2}\right)^{\frac{3}{2}})\sqrt{E} \tag{2.1}$$

Equation 2.1 shows the dense of state as a function of energy, where m is the mass of an electron and h is Planck constant. Based on equation 2.1 we can calculate the density of states in conduction band and valence band, as follows:

$$g_c(E) = ((8\sqrt{2}\pi)\left(\frac{m_n^*}{h^2}\right)^{\frac{3}{2}})\sqrt{E - E_c} \tag{2.2}$$

$$g_v(E) = ((8\sqrt{2}\pi)\left(\frac{m_p^*}{h^2}\right)^{\frac{3}{2}})\sqrt{E_v - E} \tag{2.3}$$

In equation 2.2 and 2.3, dense of states in conduction band and valence band are shown as a function of energy. m_n^* is the effictive mass of electrons and m_p^* is the efficitive mass of holes.

Based on the concept of dense of state, the Fermi- Dirac distribution function f(E) is introduced. It shows how probable an election occupies and available energy state, which has an energy state of E at T Kelvin (K).

$$f(E) = 1/(1 + e^{\frac{E-E_F}{kT}}) \tag{2.4}$$

In equation 2.4, E_F is Fermi-energy level. It shows the probablity of finding an electron at this energy level when T>0K is exactly 0.5. For different metals and semiconductors, they have different Fermi-energy level.

When a material with high work function $\Phi = E_C - E_F$ interact with a low work function material, the electron will diffuse from lower side to the higher side to make Fermi level to a same value as showed in Figure 2.1. The potential built by this electron diffusion is called contact potential. [20]

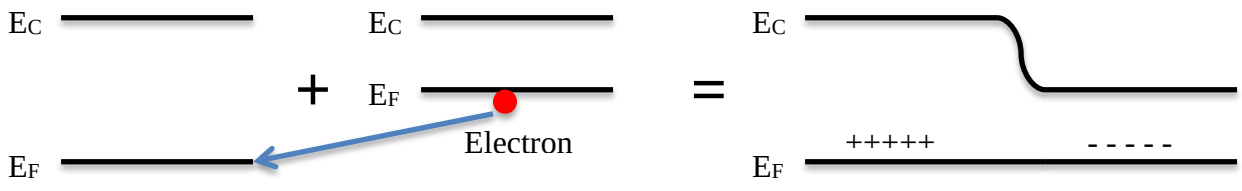

Figure 2.1. Illustration of Contact Potential

Doping is the most common method to increase the concentration of electrons or holes. For example, boron is doped into silicon in order to increase the concentration of holes. When

one boron atoms replace a silicon atom in lattice, one valence electron is missing and a hole is generated. On the other hand, arsenic is another type of dopant for creating high concentration of electron in silicon lattice. In these two cases, boron is called p-type dopant and arsenic is called n-type dopant.

2.2 P-N JUNCTION AND SOLAR CELL

2.2.1 P-N Junction

If a semiconductor is doped by n-type dopant, it is called n-type semiconductor. The semiconductor doped with p-type dopant is called p-type semiconductor. When an n-type semiconductor interacts with p-type semiconductor, the device formed by this interaction is called P-N junction. In P-N junction, the diffusion of electrons occurs from the n-type side, where the electron concentration is high, to the p-type side, where the electron concentration is low. When the electrons diffuse across the p-n junction, the recombination occurs at the p-type side, where holes are saturated. On the other hand, the charges build up on either side of the junction and create an electric field and create a diode that promotes charge flow, which is known as drift current. The drift current cancels out the diffusion current at equilibrium. [6], [7]

2.2.2 Solar Cell

Commonly, solar cells are in P-N junction type, such as traditional silicon solar cell. In P-N junction type of solar cell, the electron-hole pairs are generated and separated in the electric field

built by p-n junction. [5] When shot by photons from sunlight, the semiconductor, such as Si P-N junction layer or perovskite-structured layer in perovskite solar cell, absorbs the photons if the photon energy is higher than the band gap value of the material. The energy given to the electron by the photon excites it into the conduction band during this process. Meanwhile, the covalent bond that the electron was previously stayed at now has one electron fewer, and become as a hole. As a result, the photon absorbed by the semiconductor lattice generates a mobile electron-hole pair. Electrons move straight down to the n-contact, where the holes get blocked. On the other hand, the holes move up to the p-contact. In perovskite solar cell, the p-type material is called hole-transporting material (HTM) and n-type material is call hole-blocking layer. Possible defects in the hole-blocking layer let few holes pass through the n-type layer and recombined with the electrons before they enter the external circuit. Thus this considerably decreases solar cell efficiency.

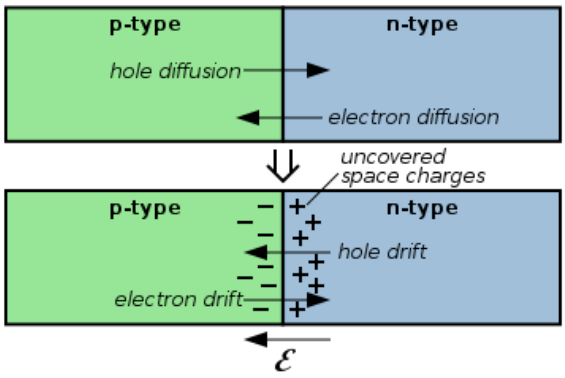

Figure 2.2. Schematic of P-N Junction Mechanism [55]

2.2.3 Space Charge Polarization

Space charge polarization happens when the ability of carrier transportation at the grain boundary is limited. Thus, the positive charge and negative charge will be concentrated at the boundary and the whole grain becomes polarized as shown in figure 2.3.

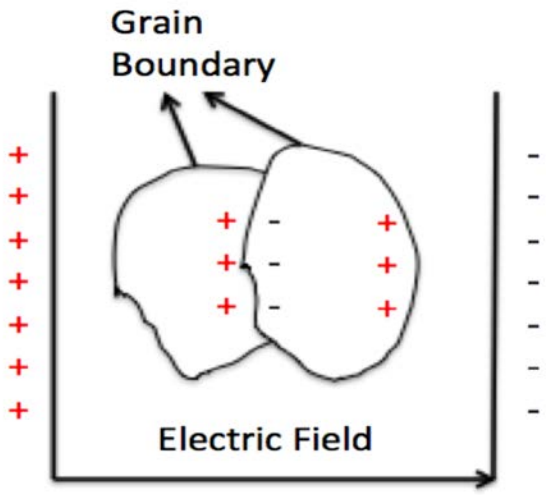

Figure 2.3. Illustration of space charge polarization

This behavior is common in multiphase materials. Since the carrier transportation ability is limited, so this behavior response to alternative current (AC) when the frequency less than 10^4Hz. [24] In P-N junction type solar cell, since n-type semiconductor and p-type semiconductor form an electric field throughout the light absorber layer, this behavior would matter if the light absorber is a multiphase material.

2.2.4 Power Convert Efficiency and J-V Curve

The power convert efficiency (PCE), also called the efficiency, of a solar cell is defined by the ratio of energy generated to electricity by solar cell from sunlight. The power generated can be described as below:

$$P = I * V = (I_L * V) - (V * I_S(e^{\frac{qV}{kT}} - 1) \quad (2.5)$$

where I_L is photocurrent, V is voltage, I is current output and I_S is saturation current.

J-V curve (Figure 2.4) is widely used to determine PCE of solar cells. The PCE is directly dependent on three factors that from J-V curves: short-circuit current density (J_{sc}), open-circuit voltage (V_{oc}) and fill factor (FF). Short-circuit current (I_{sc}), which is also known as photocurrent, presents the current of a solar cell generates when it is not linked to any external circuit. Thus, J_{sc} means short-circuit current per area. As it shows on J-V curve, the J_{sc} value equals to the current value when V=0. When I=0 on J-V curve, however, the voltage then equals to open-circuit voltage, which is the maximum voltage than generated by a solar cell.

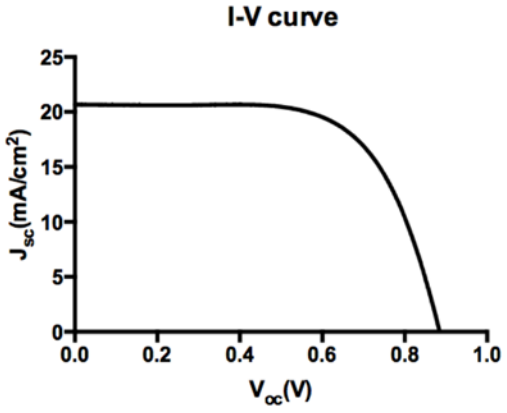

Figure 2.4. Common J-V curve of a perovskite solar cell

The fill factor (FF) is a geometric factor based on J-V curve. From J-V curve, the power generated at a specific point can be found. When considering the maximum power (P_{max}) that can be generated from a solar cell, a pair of corresponding maximum current (I_m) and maximum voltage (V_m) can be measured and $P_{max} = V_m * I_m$. Based on this relationship, FF is described as below:

$$FF = \frac{V_m * I_m}{V_{oc} * I_{sc}} \tag{2.6}$$

FF is considerable sensitive to solar cell's quality. For example, series resistance, which results from poor attaching between the surfaces of different layers in solar cell, can significantly lower the FF and eventually hinder the PCE of solar cell.

Thus, the equation of the PCE of a solar cell can be given by:

$$PCE = \frac{P_{generated}}{P_{Photon}} = \frac{V_{oc} * I_{sc} * FF}{P_{photon}} \tag{2.7}$$

2.2.5 Incident Photon-to-Current Efficiency (IPCE)

Incident photon-to-current efficiency (IPCE) is an important concept in describing the process of photo power conversion. It is defined as a ratio of the number of EHPs generated by incident photons over the number of total incident photons. IPCE is a function of the wavelength (λ) of incident photons. It increases as the number of photons absorbed by solar cell increases and the number of carriers recombined before they reach external circuit decreases. IPCE is calculated by the ratio of photogenerated electrons to incident photons, as shown in Equation 2.8:

$$IPCE = \frac{1240 * I_{sc}}{\frac{I_{photon}}{responsivity} * \lambda} = \frac{1240 * I_{sc}}{P_{incident\ photon} * \lambda} \tag{2.8}$$

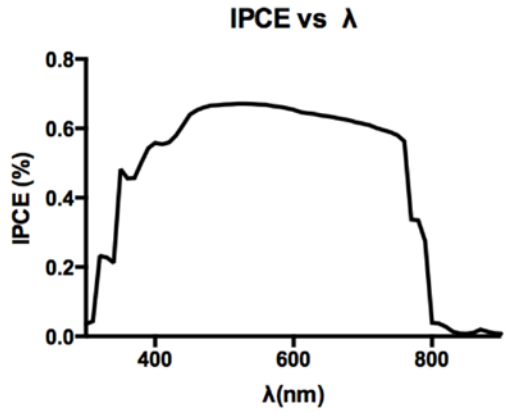

Figure 2.5. Plot of IPCE as a function of incident photon's wavelength

The integration of IPCE over whole wavelengths corresponds to I_{sc} of the solar cell. If the area of exposed to incident photon is limited, this value can be seen as short-circuit current density (J_{sc}). When IPCE is multiplied by solar radiation spectrum, the contribution of different wavelength light to I_{sc} can be found (Figure 2.6).

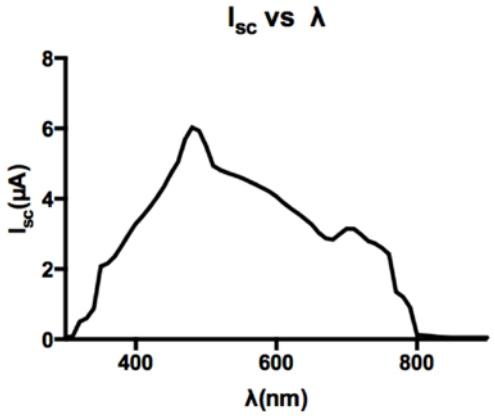

Figure 2.6. Plot of I_{sc} as a function of incident photon's wavelength

2.2.6 Carrier Recombination and Lifetime

Carrier recombination is a common behavior in semiconductor device, such as P-N junction and solar cell. When an electron in conduction band meets and combines with a hole in valence band, electrons and holes recombine and releases photon or phonon for energy compensation. Sometime this behavior happens indirectly: the electron will first be trapped by a defect or an impurity in crystal lattice. Then the trapped electron further drop down and combine with a hole in valence band. [20] As mentioned before, the recombination is harmful to the solar cell, since it decreases the PCE and IPCE of a solar cell.

The time dependence of the recombination process is related to minority carrier lifetime, which is a function of excess minority carrier concentration. For a p-type semiconductor, electron is the minority carrier. When the semiconductor is exposed to incident photon, the excess electron concentration is described as equation 2.9 below:

$$\Delta n_p = n_p - n_{p0} \tag{2.9}$$

where Δn_p is the excess electron concentration, n_p is total electron concentration and n_{p0} is equilibrium electron concentration. Consider G_{ph} is the rate of photogeneration, and recombination rate is V, so the relation of total electron concentration over time is described in equation 2.10 below.

$$\frac{\mathrm{d}n_p}{dt} = \frac{dn_{p0} + d\Delta n_p}{dt} = G_{ph} - V \tag{2.10}$$

Since n_{p0} doesn't change over time, so $\frac{dn_{p0}}{dt} = 0$. We assume that the recombination rate V is always a constant. So, the equation 2.10 can be transferred to:

$$\frac{\mathrm{d}n_p}{dt} = \frac{d\Delta n_p}{dt} = G_{ph} - \frac{\Delta n_p}{\tau_n} \tag{2.11}$$

In equation 2.11, τ_n is carrier lifetime, which indicates how long the minority carrier survives in the semiconductor. Equation 2.11 works only when the assumption of a constant recombination rate is valid.

2.3 PEROVSKITE SOLAR CELL

2.3.1 Light Absorber Perovskite

In Perovskite solar cell, the perovskite, methylammonium trihalide is act as light absorber, which absorbs incident photons and generate electron and hole pairs. Thus, this is the most important material in a solar cell.

2.3.1.1 Structure of ABX_3

The perovskite structure is named after $CaTiO_3$, which is an ABX_3 cubic structure. In this cubic crystal cell, A is located at (000) point, B is located at (½½½) and Xs are located at (½½0), (0½½) and (½0½). The most commonly studied perovskite structure that used in solar cell is methylammonium lead trihalide ($MAPbX_3$), specifically methylammonium lead triodide (MAPbI3 or $CH_3NH_3PbI_3$), where $CH_3NH_3^+$ refers to A, Pb^{2+} refers to B and X^- or I^- refers to X. This chemical compound is synthesized from reaction under room temperature between PbI2 and methylammonium iodide (MAI), which is the product from the reaction between methylamine and hydrogen iodide. The perovskite structure used in solar cell is usually unstable. Besides $CH_3NH_3PbI_3$, $CH_3NH_3SnX_3$ and $CH_3NH_3PbX_3$ are sensitive to air, moisture and other chemicals that have active hydrogen atoms like carbolic acid and alcohol. Once the perovskite structure

contact directly with these chemicals, the whole structure will decompose quickly and the efficiency of solar cell will decrease dramatically.

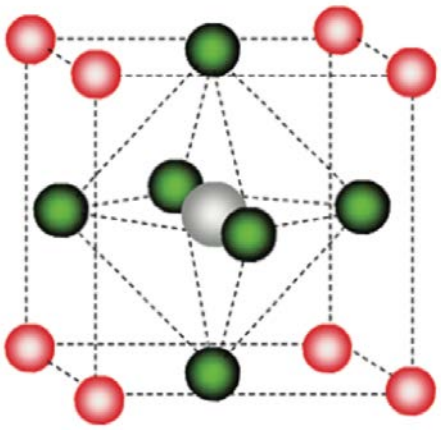

Figure 2.7. Perovskite Crystal Structure [42]

2.3.1.2 Synthesis Reaction

The $MAPbI_3$ is synthesized by the combination reaction of methylammonium iodide and lead iodide.

$$CH_3NH_3I + PbI_2 \rightarrow CH_3NH_3PbI_3 \quad (2.12)$$

Currently, there are two main methods of synthesis method: one-step method and two-step method. The most popular one-step method is called solvent engineering. [11] In solvent engineering method, researchers mixed methylammonium iodide (MAI), PbI_2 together in γ-butyrolactone to produce perovskite solution. In two-step method, [22] researchers make PbI_2 and MAI solution separately. Then use spin coating method to create PbI_2 layer on the substrate first. Later dipping the PbI_2 coated substrate in MAI solution and the perovskite is synthesized. After dip coating, the perovskite layer is heated for crystallization.

2.3.1.3 Degradation

As mentioned in 2.4.1, the perovskite is very sensitive to air and moisture. When exposed to mixture of water, oxygen and elevated temperature, the perovskite will suffer from several decomposition reactions below: [23]

$$CH_3NH_3PbI_3 \xrightarrow{Temperature} CH_3NH_3I + PbI_2 \tag{2.13}$$

$$CH_3NH_3I_{(s)} \xrightarrow{Water\ Vapor} CH_3NH_2 + HI_{(aq)} \tag{2.14}$$

$$4HI_{(aq)} + O_2 \rightarrow 2H_2O + 2I_2 \tag{2.15}$$

In order to hinder the reaction listed above moving to the right direction, the perovskite solar cell should be protected from interacting with water vapor and high concentration oxygen gas. Also, perovskite solar cell should never be heated above 90℃. Even below 90℃, the degradation of perovskite solar cell is significant over time, as shown in the figure below:

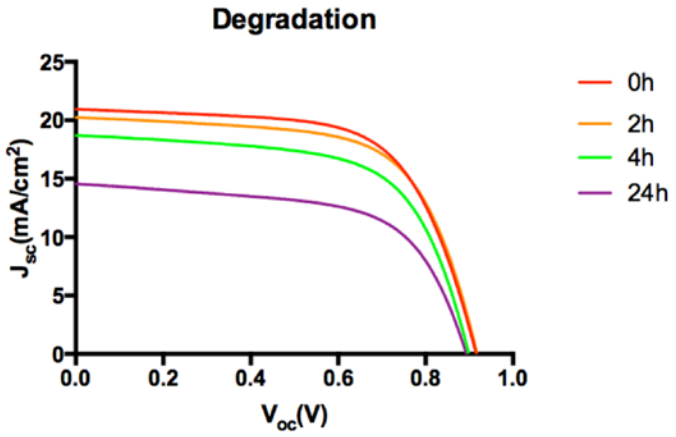

Figure 2.8. Perovskite degradation under 35% humidity and 85℃

2.3.2 Perovskite Solar Cell Development

Due to its instability, the researches into perovskite solar cell just began in recent years. In 2009, Miyasaka et al. reported the first incorporation into a solar cell. [8] The paper was focused on dye-sensitized solar cell architecture, and eventually obtained a power conversion efficiency of 3.8%. In this research, a thin layer of perovskite on mesoporous TiO2 was used as light absorber, which pretty much like the perovskite layer structure that people commonly use currently. However, due to the use of a liquid corrosive electrolyte, the cell was only stable for minutes. At this time, how to find a substitution of the liquid corrosive electrolyte is a main topic, because perovskite is unstable under air and moisture condition. Besides, the fabrication process needed to avoid airflow, especially oxygen, water moisture and high temperature, since methylammonium lead trihalides will decompose at above 90℃. As a result, the major technical barrier in perovskite solar research is how to figure out a proper fabrication method in order to preserve the perovskite structure during the process. In 2011 Park et al. improved the process using the same dye-sensitized concept and achieving 6.5% power conversion efficiency. [9]

In 2012, a breakthrough came. Henry Snaith and Mike Lee from the University of Oxford realised that the perovskite was stable if contacted with a solid-state hole transporter such as Spiro-OMeTAD and did not require the mesoporous TiO2 layer in order to transport electrons. [10] They got the power conversion efficiency about 10%. Another architecture by using the activated TiO2 with Spiro-OMeTAD showed that efficiency of almost 10% was achievable. By replacing solid-state hole transporter with an inert scaffold, higher efficiencies, above 10%, were got. [11] Further experiments in replacing the mesoporous TiO2 with Al2O3 resulted in increased open-circuit voltage (V_{OC}) and a relative improvement in efficiency of 3-5%. [12]

In 2013, the research in perovskite solar cell boosted up and resulted in many achievements. Burschka et al. demonstrated a deposition technique for the sensitized architecture exceeding 15% efficiency by a two-step solution processing. [13] At almost the time Liu et al. showed that it was possible to fabricate perovskite solar cells by thermal evaporation, with efficiency more than 15%. [14] Docampo et al. also showed that it was possible to fabricate perovskite solar cells in the typical 'organic solar cell' architecture, an 'inverted' configuration with the hole transporter below and the electron collector above the perovskite planar film. [15]

In 2014, a range of new deposition techniques with resulted in even higher efficiencies were reported. Yang Yang at UCLA claimed a reverse-scan efficiency of 19.3% by using the planar thin-film architecture. [16] Later on a device by researchers from KRICT achieved a new record with the certification of a non-stabilized efficiency of 20.1%. At the 6th World Conference on Photovoltaic Energy Conversion in Kyoto, Japan, the achievement of a single-junction perovskite solar cell with a power-conversion efficiency of 24% was mentioned.

In 2015, the researches in perovskite solar cell continue growing rapidly. Im J H et al introduced nanowire structured methylammonium lead triodide used in the perovskite solar cell, with open-circuit voltage (V_{OC}) above 1 volt and efficiency of 14.71%. [17] Besides, many other works is being reported soon.

Perovskite solar cell is still in lab research stage and is not available on the market. However, since they have low cost and easy to fabricate, they will to some extent increase the penetration rate of the use of solar cell. Currently, many places in the world, where the sunlight intensity is high and suitable for using solar cell, do not build solar cell power plant because of silicon solar cell’s high cost. Perovskite solar cell is the perfect solution to this problem. The low cost also results in low price that make the perovskite solar cells attractive for domestic use.

Besides, perovskite solar cell may have many other applications that will be discovered after it comes to the market. The start-up companies have already promised making modules on the market by 2017. By that time, the perovskite solar cell will change the world in its ways.

2.3.3 Structural Types of Perovskite Solar Cell

As a type of P-N junction solar cell, perovskite solar cell is a combination of P-N junction, light absorber, anode and cathode. The hole blocking layer, also called electron transporting layer (ETL), plays the role of n-type semiconductor. Most commonly, it is made of TiO2 by titanium isopropoxide (TTIP) in 1-butanol solution, where TTIP is a precursor of TiO_2. The anode, which is linked tightly to n-type semiconductor, transports electrons to external circuit. Fluorine doped tin oxide (FTO) and indium doped tin oxide (ITO) on glass substrate are two kinds of material that used as the anode in perovskite solar cell. The p-type semiconductor is commonly Li^+ doped Spiro-OMeTAD or non-doped tetrathiafulvalene derivative (TTF-1). [18] Above the p-type material, the cathode, usually gold, is deposited because of its good conductivity and Fermi energy level. Light absorber, the perovskite material is located between the n-type layer and the p-type layer. Perovskite is usually deposited in the mesoporous scaffold layer, which plays a role of electron transport material. TiO_2 is the most commonly used as the mesoporous scaffold layer for its high transparency and conductivity. Based on different TiO_2 scaffold structure, three structural types of perovskite solar cell are distinguished: planar, nanoparticle based and nanowire based solar cell.

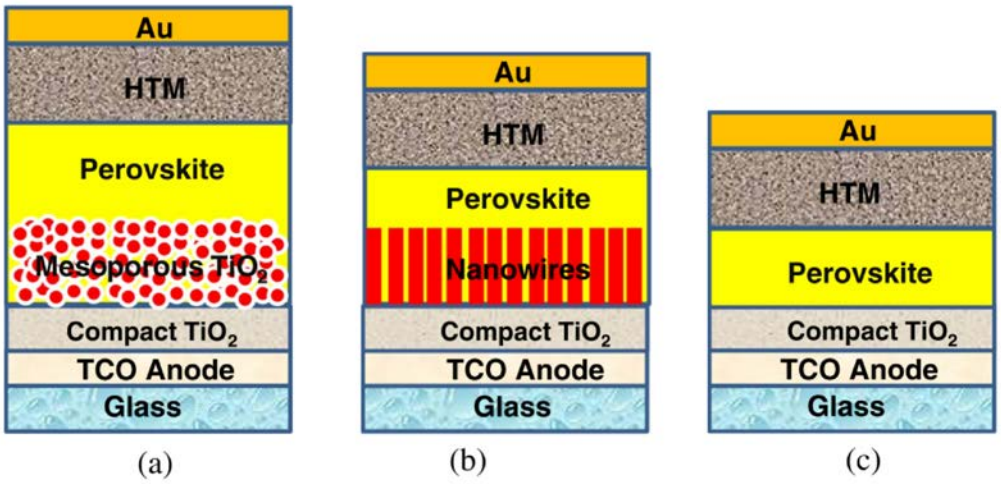

Figure 2.9. Three structural types of perovskite solar cell: (a) TiO_2 nanoparticle based; (b) TiO_2 nanowire based; (c) Planar structure

In order to prevent the current leakage, one edge of FTO substrate is etched by acid to remove the conductive FTO layer from the glass. This edge is called etching side in experiment. On the other paralleled edge, the FTO is exposed out without any single layer coated for building the anode. This side is called FTO side in this thesis. The structure is shown in the figure below.

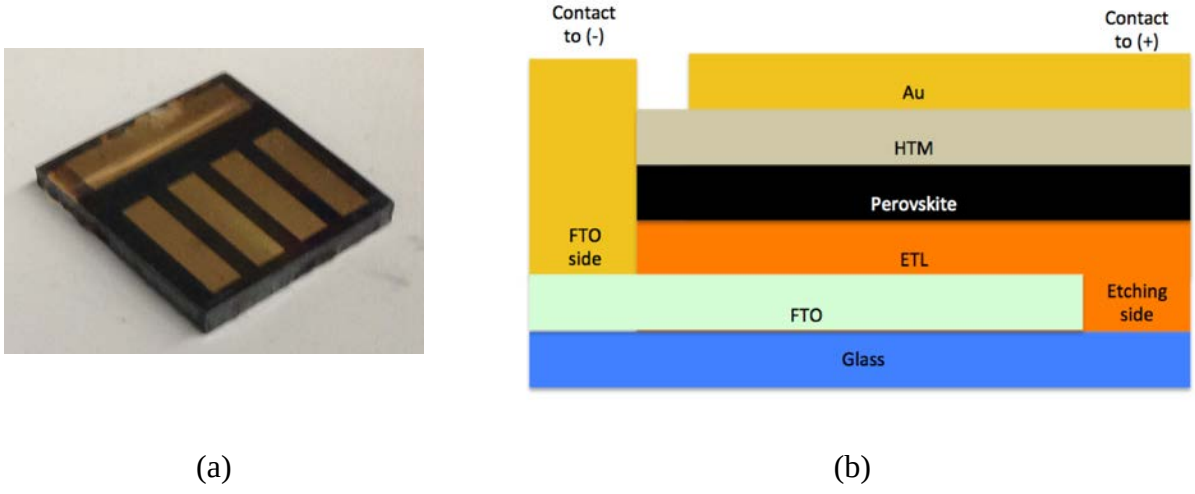

Figure 2.10. Perovskite solar cell structure (a) Photo of perovskite solar cell (b) schematic figure

2.3.3.1 Nanoparticle Structure

The nanoparticle structure is currently the most common structure for the perovskite solar cell where the perovskite crystalline is deposited in TiO_2 mesoporous layer and functions as a light absorber. As figure 2.9(a) shown, perovskite first infiltrated in the mesoporous structure, and then formed pure perovskite cuboid structure on top of the nanoparticle layer. [34] The open-circuit voltage and fill factor of perovskite solar cell decrease as the TiO_2 nanoparticle film thickness increases [11] Because the resistance of TiO_2 nanoparticle is lower than the perovskite, the overall conductivity increases due to the presence of TiO_2 nanoparticle.

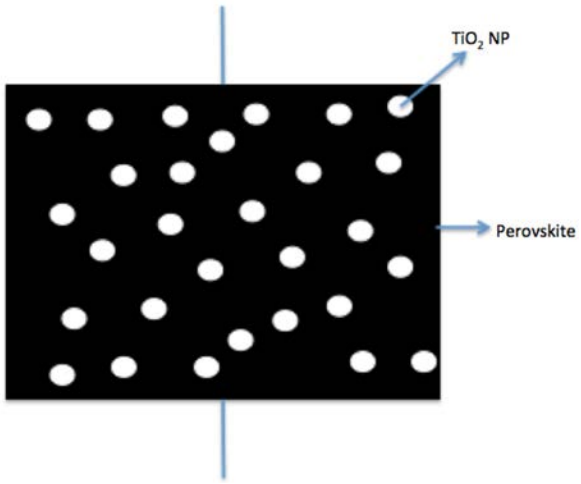

(a)

$$\rho = \rho_c \frac{1 + 0.5\chi_d}{1 - \chi_d}$$

(b)

Figure 2.11. Nanoparticle dispersed model (a) Illustration of the model (b) corresponding equation: ρ_c refers to resistivity of continuous phase and χ_d refers to volume ratio of dispersed phase

In figure 2.11(a), the perovskite plays the role of continuous phase and TiO_2 nanoparticle is the mesoporous phase. As a result, in the equation of figure 2.11(b), the resistivity is decreased.

It has been reported that the mesoporous TiO_2 sensitized layer with the perovskite absorber shows UV light induced instability. This is due to the interaction between photo-generated holes inside the TiO_2 and oxygen radicals on the surface of TiO_2. [19]

2.3.3.2 Nanowire Structure

As shown in figure 2.9(b), the TiO_2 nanowire grow perpendicular to the compact TiO2 and HTM layers on the substrate. Photovoltaic performance of TiO_2 nanowire based perovskite solar cell depends greatly on the nanowire's length. Open-circuit voltage decreases with nanowire length increases and results in power convert efficiency decreases. However, the carrier recombination behavior remains similar when nanowire length changes. [43]

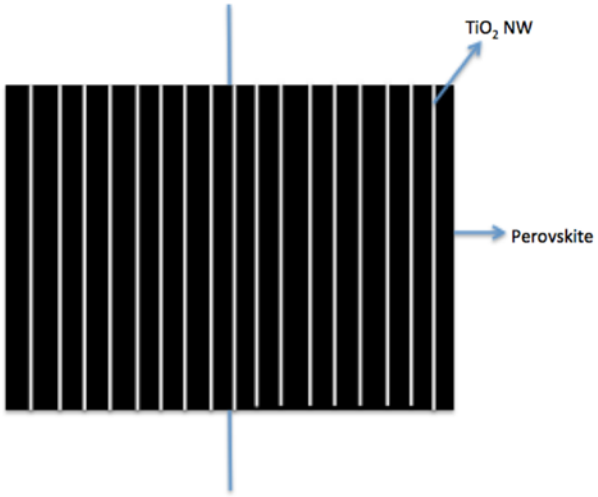

(a)

$$\sigma_{eff} = \chi_\alpha \sigma_\alpha + \chi_\beta \sigma_\beta$$

(b)

Figure 2.12. Nanowire (nanorod) mixture model: (a) Illustration of the model (b) corresponding equation: $\boldsymbol{\sigma_{eff}}$ refers to overall conductivity; $\boldsymbol{\sigma_\alpha}$ and $\boldsymbol{\sigma_\beta}$refers to conductivity of α phase and β phase; $\boldsymbol{\chi_\alpha}$ and $\boldsymbol{\chi_\beta}$refers to volume ratio of α phase and β phase

Figure 2.12 shows how the presence of nanowire phase changes the overall conductivity of the light-absorber layer in perovskite solar cell. The large volume ratio of TiO_2 nanowire, the higher conductivity the layer is. However, if the attaching between nanowire and perovskite is poor, it will cause low transport ability of carriers and the conductivity will increase dramatically.

2.3.3.3 Planar Structure

As shown in figure 2.9(c), planar structure perovskite solar cells contain no TiO_2 nanostructure for scaffold and cuboid-structured perovskite crystal deposit directly on the n-type electron-transporting layer. In this case, the solar cell's property is highly dependent on the coverage of perovskite layer (>90%) on the substrate. [44] This film is extremely sensitive to moisture before fully recrystallized, thus, this layer is prepare in dry nitrogen ambiance.

Since TiO_2 and other TCO material are not mixed in the light-absorber layer, the planar structure perovskite solar cell does not have an advantage of conductivity compared to TiO_2 nanoparticle and nanowire perovskite solar cell. Perovskite layer is formed by crystalline grains, and is placed between n-type and p-type semiconductor, which produce an electric field as shown in Figure 2.2. As a result, space charge polarization behavior, as shown in figure 2.3, is relatively significant in planar perovskite solar cell.

2.3.4 Titanium Oxide Nanowire Fabrication

Found in nature, titanium oxide has three different structural forms: rutile, anatase and brooklite, where rutile and anatase have a tetragonal structure while brooklite has an orthorhombic structure. Among all TiO_2 nanowire (NW) or nanorod (NR) fabrication methods that have been published so far, hydrothermal method is the most commonly used method. [26][27][28] It has

the advantage of easier controlling nanowire's length and better array distribution. [26] Usually, hydrothermal method produce pure rutile nanorod, however, anatase and brooklite nanorod can also be produced by selective synthesis route. [29][30] In this thesis, hydrothermal method is used to fabricate rutile TiO_2 nanowire.

2.3.4.1 Mechanism

TiO_2 nanowire growth is strongly depended on rutile's inherent growth behavior and hydrothermal preparation conditions. [27] The TiO_6 octahedral structure linked as a polymer chain along c-axis. [31] For rutile TiO_2, in the polymer chain, each octahedron connect with another through the point of oxygen by chemical bonds, which means the bonding in the chain is stronger than interaction between chains. Theoretically, the stronger the chemical bond, the faster the crystal growth. [32] Thus, the growth rate in [001] direction of rutile TiO_2 nanowire has a growth rate far higher than [110] direction. [31] The formation reaction of TiO_2 nanowire is by dehydrating the monomer of $[TiO(OH_2)_5]^{2+}$. The monomer $[TiO(OH_2)_5]^{2+}$, however, is formed by precursor TTIP, which is $Ti(OCH_3)_4$. The chemical equations are shown as below.

$$Ti^{4+} + 6H_2O \rightarrow [TiO(OH_2)_5]^{2+} + 2H^+ \quad (2.16)$$

$$[TiO(OH_2)_5]^{2+} \xrightarrow{dehydration} TiO_2 + 4H_2O + 2H^+ \quad (2.17)$$

Because hydrogen ions are produced, so high concentration HCl are introduced in this reaction as inhibitor of nanowire growth.

Compared with homogeneous nucleation, crystalline phase's heterogeneous necleation is easier. [33] As a result, before TiO_2 nanowire deposition, a thin layer of TiO_2 nanocrystalline should be coated on the substrate and got annealed. Thus, these nanocrystalline particles would

be seen as seeds of heterogeneous nucleation. Meanwhile, the well-distributed seeds would make nanowire arrays well aligned also, for their crystal structure matches each other. [27]

2.3.4.2 Effects of different factors

In hydrothermal method, many parameters have been proved to be useful for controlling TiO_2 nanowire product's length, density and aspect ratio. [21], [26] As a result, hydrothermal method can produce varies of TiO_2 nanowire substrate with totally different lengths and densities. However, on the other hand, from experimental point of view, reproducing the same product under similar conditions is hard to achieve.

Growth time is one of the most important parameters of TiO_2 nanowire growth. In principle the longer the growth time, the longer the TiO_2 nanowires are. However, the relation between length and time is not completely linear. At 150℃, no TiO_2 nanowires were found on FTO substrate when growth time was less than 3h. The nanowire length reached 600nm after 4h of growth and 2μm after 20h. Meanwhile, the diameter of nanowire increases. [26] When the growth time is near to the time for the reaction reaches equilibrium, the nanowire product is easy to be peeled off the substrate. [26] So the solution state during the growth should remain supersaturated by the titanium precursor. If not, the competing reactions of crystallization and dissolution will make the nanowire fragile.

Growth temperature is another parameter that has a positive relationship to nanowire length. When the temperature is less than 100℃, no nanowire was found on substrate. When the temperature increases from 150℃ to 200℃, the growth rate increases by a factor of 5. [26] Since as temperature increase, the reaction rate increases. [35] At high temperature, the time needed for nanowire growth reaction to reach equilibrium is shorter and the peeling effect become significant. [26]

In chapter 2.3.4.1, the effect of acid, in principle hydrochloric acid (HCl) was mentioned. When the pH is extremely low, the reaction will be suppressed by high concentration of H^+. As a result, HCl is the inhibitor of TiO_2 nanowire growth reaction.

The concentration of precursor, in principle TTIP, is related to the concentration of nucleation in the reacting solution. The increasing in precursor concentration will increase the nanowire length when the reaction time is fixed. However, this increase contains both heterogeneous nucleation and homogenous nucleation. In homogeneous nucleation, TiO_2 is formed in the solution instead of on substrate and nanowire do not grow. Thus, experimentally, the solution becomes turbid if the concentration of precursor is extremely high. On the substrate, the nanowires have a high possibility to run into neighboring nanowire and stop growing. [26] When the concentration of precursor is low, on the other hand, the nanowire grows to a longer length because the risk of running into the neighbor is decreased.

In addition to TTIP, many kinds of precursors are used in hydrothermal method. $TiCl_4$, titanium butoxide can also act as the precursor of TiO_2 nanowire growth reaction. [26]

3.0 RESEARCH DESCRIPTION

3.1 HYPOTHESIS

The primary hypothesis of this thesis is that the electron transporting behavior in the light-absorbing layer of TiO_2 nanowire based perovskite solar cells are different as TiO_2 nanoparticle based solar cells. The space charge polarization effects in TiO_2 nanowire based perovskite solar cells matters more than that in TiO_2 nanoparticle based solar cells and thus frequency dependence of NW based cell is higher than NP based cell. The secondary hypothesis is the carrier lifetime in NW based cell is different from NP based cell and this has effects on frequency dependence when the frequency is high.

3.2 OBJECTIVES

The purpose of this thesis is to describe and explain the differences in electron transporting behaviors in perovskite solar cell (PSC) based on internal polarization effects by comparing photovoltaic properties between TiO_2 nanoparticle and nanowire based perovskite solar cells, using I-V, IPCE and carrier lifetime measurement.

3.3 TASKS

The first task of this thesis is fabricating consistent TiO_2 nanowire substrate with nanowire length in the range of 200 to 600nm. The second task is making both TiO_2 nanoparticle and nanowire based perovskite solar cells with good properties, which can reach the property in previously reported paper. The third task is doing both static and dynamic photovoltaic measurements in order to study the behaviors of electron transportation in perovskite solar cell.

4.0 EXPERIMENTAL DETAILS

4.1 TITANIUM OXIDE NANOWIRE GROWTH

In this thesis, hydrothermal method is used for TiO_2 nanowire growth experiment. The heating method is using microwave oven (Mars 6) to generate heat inside the Teflon vessel where the substrates are immerged into the solution. The temperature and pressure are controlled in the control vessel where contains the same volume of solution as the vessels used for reaction.

The pure rutile TiO_2 nanowires are grown on titanium oxide coated FTO (NSG TEC^{TM} 15, 15Ω/sq) substrate in order to increase the trend of heterogeneous nucleation. The titanium oxide layer (~5μm) is coated on the substrate by spin coating. Soft baking and annealing are necessary after spin coating. The solution is made by dissolving 0.46ml TTIP (Sigma-Aldrich, A00133) in 7.2μL HNO_3 (70%) acidized 13ml ethanol (200proof). The spin coating condition is 3000rpm for 30s. Since this layer is also used as hole blocking layer, the FTO side on is taped by 5mm thick Kapton tape in order to prevent TTIP deposited on FTO insulating the FTO side. The soft baking condition is 100℃ for 10min. The annealing condition is 500℃ for 30min.

The solutions of reaction were prepared by dissolving hydrochloric acid (Fisher Scientific, A00139) in deionized (DI) water at room temperature to certain concentrations. The total volume of HCl solution is fixed to 120ml. The concentration changes by the ratio of HCl and water. After stirring for 10min, 1.7ml TTIP (Sigma-Aldrich, A00133) precursor is added in the solution

and stirring for 15min. Because the reaction temperature and acidity are too high for Kepton tape, so the FTO side is covered by Teflon tape instead of Kepton tape in order to prevent the solution interact with FTO side and deposit TiO_2 nanowire on the FTO side.

Table 4.1. TiO2 nanowire growth condition

Condition Number	Volume of HCl (ml)	Volume of DI water (ml)	Volume of TTIP (ml)	Growth Time (min)	Growth Temperature (℃)
1	67	53	1.7	15	160
2	67	53	1.7	30	160
3	67	53	1.7	45	160
4	67	53	1.7	30	180
5	67	53	1.7	30	190
6	67	53	1.0	30	160
7	67	53	2.0	30	160
8	40	80	1.7	30	160
9	40	80	1.0	30	160
10	40	80	2.0	30	160
11	80	40	1.7	30	160
12	80	40	1.0	30	160
13	80	40	2.0	30	160

The total growth conditions studied are listed in table 4.1 above, including the parameters of time, temperature, acidity and precursor concentration. The substrates are mounted evenly on plastic holders and immerged into the solution in Teflon vessels. Each vessel contains three substrates. One of the three substrates is used for checking nanowire length via scanning electron microscope (SEM). The other two are used for perovskite solar cell fabrication if the nanowire length and feature fits the expectation. The ramping time and cooling time for microwave heating session are fixed to 30min and 5min. After the heating, the substrates are taken out and washed by DI water and ethanol. Annealing (500℃ 60min) is done after washing and drying of the substrate.

4.2 PEROVSKITE SOLAR CELL FABRICATION

As the main object in this thesis, perovskite solar cells are fabricated from the first step. This chapter shows the fabrication steps of TiO_2 nanoparticle based perovskite solar cell, or called reference perovskite solar cell. Followed reported paper, two-step spin coating method is used in the experiment. [34]

4.2.1 FTO Substrate Preparation

With high conductivity, the NSG TEC^{TM} 8 FTO substrates were chosen as the substrate for TiO_2 nanoparticle based perovskite solar cell fabrication. The resistivity is 8Ω/sq, relatively lower than TEC 15 substrate used in TiO_2 nanowire based perovskite solar cell. First, a 12inch×12inch FTO glass pad was cut into 2cm×2cm sized substrates. Each substrate was etched by Zn powder plus

1:1 HCl (Fisher Scientific, A00139): DI water solution to form a 4mm wide etching side. The substrates were washed by acetone, DI water and ethanol (190proof) for 15min in each solvent.

4.2.2 N-Type Hole Blocking Layer

After washed in ethanol solvent, the substrates were taken out and dried by airflow. Kepton tape was used to cover a 2cm in length and 5mm in width area parallel to the etching side to prevent this area, which is used as anode, coated by n-type material. Spin coating method was used in this experiment for material coating. The solution is 0.5 mol/L titanium diisopropoxide bis(acetylacetonate) in 1-butanol. This solution is also called 1-butanol solution. Spin coating condition is 40 μL solution, 3000 rpm for 30 s. Soft baking condition is 100℃ for 10 min and annealing condition is 500℃ for 30 min.

4.2.3 $TiCl_4$ Treatment

$TiCl_4$ treatment is a kind of water phase treatment. [41] The treatment solution is made by 80ml DI water and 2ml 2M $TiCl_4$ solution, which is made by dissolving $TiCl_4$ (Sigma-Aldrich, >98%) in froze DI water. This treatment can make the surface of hole blocking layer flatter and filled pores that are formed during the spin coating of hole blocking layer solution. The treatment condition is 72℃ for 30 min. After the treatment, substrates are washed by DI water and ethanol. Post-annealing condition is 500℃ for 30 min.

4.2.4 Titanium Oxide Mesoporous Layer

By dissolving TiO_2 nanoparticle paste (Dyesol) into ethanol (200proof), the TiO2 mesoporous solution with weight ratio of 1:5.5 (TiO_2: EtOH) is made. This layer is also formed by spin coating method with the condition of 40 μL solution, 3000rpm for 30s. The estimation of layer's thickness is 200 nm. Since no tape is used to cover the FTO side, a trimming step is used to remove the TiO_2 coated on the FTO side after spin coating. Soft baking condition is 100℃ for 10min and post-annealing condition is 500℃ for 30 min.

4.2.5 Two Step Perovskite Fabrication

In two-step fabrication method, PbI_2 and Methylamine Iodide (MAI) are deposited on the substrate separately. PbI_2 (Sigma-Aldrich, >99%) is dissolved in DMF (Sigma-Aldrich, >98%) to form a 1mol/L concentration solution. MAI is dissolved in isopropanol (Sigma-Aldrich, 95%) and the concentration is 7 mg/ml. The dissolving condition for PbI_2 solution is heating at 85℃ for 30 min and MAI solution is just manually shaking because MAI has very low heat resistance. The spin coating process is first coating 40 μL PbI_2 solution at 4000 rpm for 30 s. Then use soft baking at 55 ℃ for 3min and 100 ℃ for 6 min. After air-cooled, the sample is coated by 250 μL of MAI solution on the condition of 0rpm for 40 s and 4000 rpm for 20 s. The soft baking condition after spin coating is 100 ℃ for 10 min.

4.2.6 Hole Transporting Material

The hole transporting material used in this experiment is 1% Li^+ doped spiro-OMeTAD. [36] Spiro-OMeTAD produces a structure to transport holes and Li^+ increases conductivity. This material is coated on perovskite substrate by spin coating method. Adding 0.18 g Li-TFSI (Sigma-Aldrich) in 0.25 ml acetonitrile solution 8.8 μL (Sigma-Aldrich) into 36 mg Spiro-OMeTAD (Lumtec) in 0.5 ml chlorobenzene (Sigma-Aldrich) makes the solution. 14.4 μL 4-tert-butylpyridine (TBP) was also added. The spin coating condition is 4000 rpm for 30 s. No soft baking needed because the perovskite will decompose if soft baking time is too long.

After the spin coating, a trimming step is added in order to remove the perovskite and HTM coated on FTO side.

4.2.7 Au Deposition

Au is used to form the electrodes on the solar cell. It both deposited on perovskite region to form cathode and deposited on FTO side to form anode. This layer is deposited by electron beam deposition method where high intensity electron shoots on a crucible contains target metal. [40] At very low pressure ($<5\times10^{-6}$ Torr), the metal will be generated by high intensity electron beam and deposited evenly on the holder, where the samples mounted, inside the chamber. Since this method can cover all areas, a mask with electrode pattern is used to cover the sample and expose the electrode area. The deposition rate is 0.05 nm/s and a final thickness is 80 nm.

4.2.8 Difference in Fabrication Between NP based and NW based Perovskite Solar Cell

This chapter in principle illustrates the fabrication procedure of NP based perovskite solar cell. For NW based perovskite solar cell, the fabrication has little difference compare to NP based cells. First, the types of FTO are different: NP based use TEC8, which has higher conductivity while NW based used TEC15, which has higher transmittance. Second, NP based cells use 1-butanol layer solution, but NW based cells use TTIP in 1-butanol solution. At last, the procedure of NW based cell is substrate preparation, TTIP solution coating, NW growth, $TiCl_4$ treatment, perovskite coating, HTM coating and Au deposition, which is a little different from NP based cell.

4.3 ULTRAVIOLET-VISIBLE MICROSCOPY

Ultraviolet-visible (UV/Vis) microscopy was used to measure the absorbance and transmittance of FTO substrate, TiO_2 deposited substrate and perovskite solar cell. The UV source generated light and split by monochromator. The samples were mounted on the light path and absorbed a ratio of photons when the light passed through. The detector measured the remaining photons by measuring the power of light loss and output the signal. [39] Before the measurement, a no-sample run should be made for collecting the reference data, so that the loss of power due to the sample can be calculated. The number of photons loss or absorbed by the sample is positive related to the power loss.

Two types of data curves can be obtained from UV/Vis microscopy. One is transmittance over the wavelength of incident photon and the other is absorbance over the wavelength.

Transmittance (%T) is equal to the ratio of remaining light intensity (I) and intensity of light without sample (I_0), as shown in equation 4.1. The absorbance (A), however, is calculated based on transmittance, as shown in equation 4.2.

$$\%\mathrm{T} = \frac{I}{I_o} \tag{4.1}$$

$$A = -\log\left(\frac{\%T}{100\%}\right) = -\log(\frac{I}{I_o}) \tag{4.2}$$

The Schematic figure of UV/Vis microscopy is shown below:

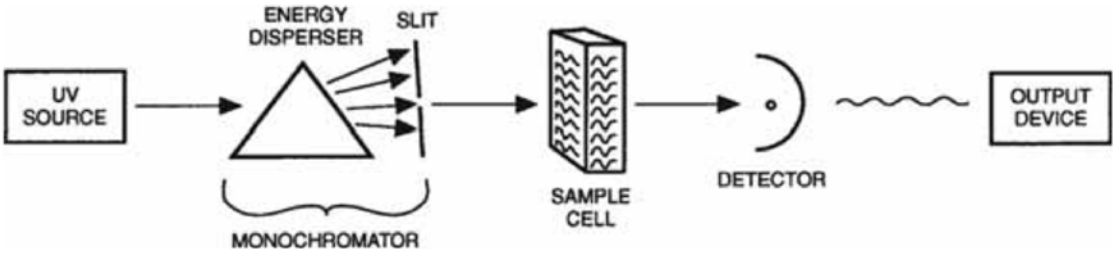

Figure 4.1. Schematic figure of UV/Vis microscopy [39]

4.4 SCANNING ELECTRON MICROSCOPE

In this experiment, scanning electron microscope (SEM) is used to check the cross-section structure of perovskite solar cell sample, top view of TiO_2 nanostructure and measure the nanowires length from cross-section view. Two SEMs were used in this experiment: Raith-EBL and FEI-XL30. Raith-EBL was selected to check the microstructure because it has higher resolution and can hold higher magnification. Since operating procedures of FEI-XL30 is simpler, it is used to briefly measure the nanowires' length. The acceleration voltage of Raith-

EBL is 15KV and FEI-XL30 is 10KV. Typical examples of both SEMs are shown in Figure 4.2 below.

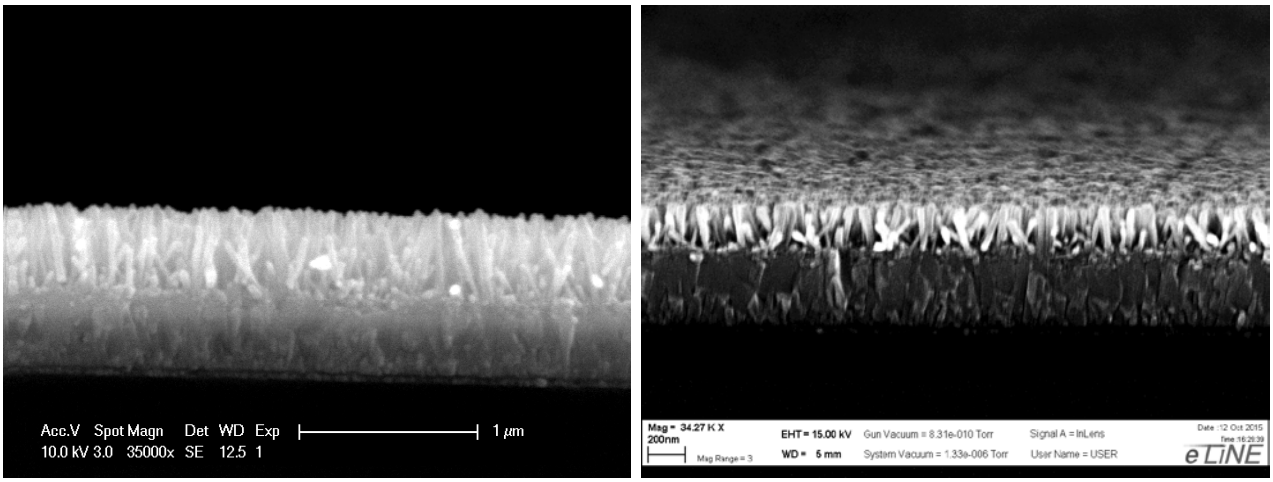

(a) (b)

Figure 4.2. Typical SEM images of TiO_2 nanowire substrate from two SEMs: (a) FEI-XL30; (b) Raith-EBL

From the SEM images, the nanowire length, width, aspect ratio and feature can be measured. The brightness is controlled manually. Regions have similar brightness are the same material for the similar conductivity. The darker regions' color, the higher conductivity they are. In Figure 4.2(b), the FTO region has darker color because it has higher conductivity compared to TiO_2 nanowire.

4.5 I-V CURVE MEASUREMENT

Solar simulator was used to measure J-V curve of perovskite solar cell sample. It can generate sunlight, which contains ultraviolet, visible and infrared light, with different intensity. [37] Since the photocurrent generated by solar cell is a function of incident photon intensity, in order to measure the photocurrent generated under 1 sun's intensity, the light intensity of solar simulator should be calibrated. The 1 sun intensity refers to standard illumination at AM1.5G. [38] The calibration is done by measure the J-V curve of silicon reference solar cell at 1 sun intensity and measure under the solar simulator to obtain another J-V curve. By comparing these two J-V curves, the light intensity of solar simulator can be calculated. The reference J-V curve under 1 sun is shown in figure 4.3.

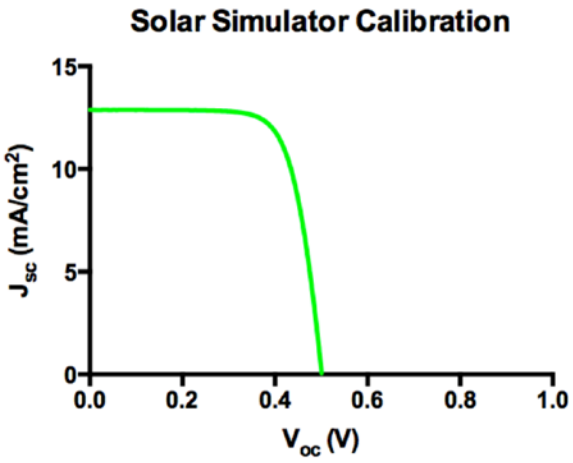

Figure 4.3. The J-V curve of silicon reference solar cell during calibration

The samples were mounted in I-V holder during the measurement, which has conductive junction points, can link to the electrode on perovskite solar cell sample. The junction points are

also linked to electrical measurement sensor and computer, thus the data can be obtained. The area on solar cell is fixed by a metal mask for the calculation of photocurrent density J_{sc} from photocurrent I_{sc}, which is directly measured from I-V curve measurement. The exposed area is $0.14cm^2$. During the measurement, the mask is covered on the sample and exposed area is on the top of electrodes. The corresponding J_{sc}, V_{oc} and FF are calculated from the curves.

4.6 IPCE MEASUEREMENT

Incident photon-to-current efficiency (IPCE) is used to measure the photocurrent generated by perovskite solar cell under different wavelength. The monochromator is used to split light from Xeon lamp to certain wavelength. The wavelength is continuously changing during the measurement in order to obtain photocurrent data in a range. The sample was mounted in light path. Anode and cathode were linked to the detector with a cable. The detector can read photocurrent data and transfer to computer.

There are two modes in IPCE measurement, alternative current (AC) mode and direct current (DC) mode. In DC mode, the single wavelength light shoots on solar cell directly. However, in AC mode, a spinning shutter is added between solar cell and light source. The spinning frequency can be changed from 1Hz to 99Hz. In this thesis, 1Hz, 10Hz, 30Hz, 50Hz, 75Hz and 95Hz are used to study the frequency dependence of the IPCE curve of NP and NW based perovskite solar cell.

When the AC mode IPCE works at a low frequency (~1Hz), the photocurrent can reach steady-state value in shutter's time interval between its open and close. As the frequency increases, the time interval is no longer enough for photocurrent to reach steady state and thus

the photocurrent value is decreased. As a result, the curve's shape in AC mode IPCE can be slightly changed when the frequency is high. [49]

4.7 ELECTRON LIFETIME MEASUREMENT

Electron lifetime measurement is introduced to measure photogenerated electron lifetime in the solar cell. Two methods are commonly used to characterizing electron lifetime: open-circuit voltage decay (OCVD) [50] and stepped light-induced transient measurement of photocurrent and photo voltage (SLIM-PCV). [51], [52]

OCVD is measuring the electron lifetime of solar cell as a function of open-circuit voltage. The solar cell sample was exposed to a light that generated by function generator. The steady-state illumination was turned off and the Voc decay curve was obtained by oscilloscope. This decay is continuous as a function of time and the relationship between Voc decay and lifetime is shown below.

$$\tau_n = -\frac{k_B T}{e}\left(\frac{dV_{oc}}{dt}\right)^{-1} \tag{4.1}$$

Equation 4.1 describes in a common nonlinear cases, electron lifetime is a function of the reciprocal of derivative of the open-circuit voltage over time under the decay condition.

SLIM-PCV is measuring the change of photocurrent and V_{oc} as a function of light intensity. The light was generated by a laser diode. The light intensity was adjusted by a set of neutral density (ND) filler, which was placed between the light source and solar cell sample. Synchronized with the function generator, the voltage transient signal was obtained by

oscilloscope and current transient signal was first converted to voltage signal by a current amplifier, and then obtained by oscilloscope.

SLIM-PCV measurement can obtain both electron lifetime and diffusion coefficient. The relationship between diffusivity (D) and exponential decay time constant (τ_c) is shown in the equation below.

$$D = \frac{L^2}{2.77\tau_c} \tag{4.2}$$

L refers to the thickness of electrode. The electron density is related to the equation below.

$$n(t) = Aexp\frac{-t}{\tau} \tag{4.3}$$

A refers to Δn, which means the difference of electron density difference before and after light intensity change. [51] When the change of light intensity is small, V_{oc} is proportional to equation 4.3. As a result, the carrier lifetime can be obtained by calculating the V_{oc} decay's relaxation time.

5.0 RESULTS AND DISCUSSION

In this chapter, SEM images of TiO_2 nanowire is shown to present the nanowire length and features under different growth condition. The results from both static and dynamic photovoltaic measurement are shown. Static measurement includes J-V curve, UV/Vis spectroscopy and DC mode IPCE. Dynamic measurement includes AC mode IPCE and carrier lifetime measurement. The structural different between NP and NW based cell will also be shown by SEM images.

5.1 NANOWIRE GROWTH RESULT

By organizing growth conditions in table 4.1, different samples can be split regarding to different parameters. Parameters including Acidity, precursor concentration, growth time and temperature, which discussed in chapter 2.3.4.2, are studied in these experiments.

5.1.1 Acidity

By taking condition No.2, 8 and 11 together, the effect of parameter of acidity can be shown. Figure 5.1 shows the TiO_2 nanowire substrate at different pH.

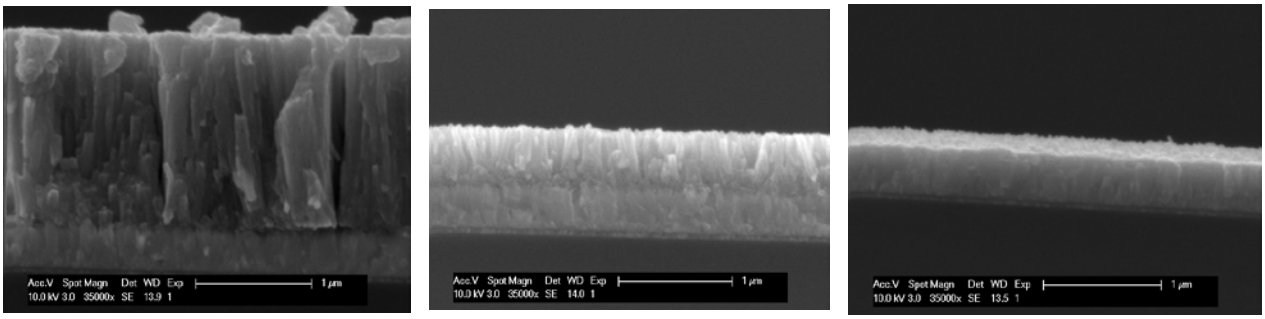

(a) (b) (c)

Figure 5.1. The effect of acidity on TiO_2 nanowire length: (a) condition No.8: 40ml HCl; (b) condition No.2: 67ml HCl; (c) condition No.11: 80ml HCl

TiO_2 nanowire length increase as the amount of HCl decreases, because HCl is an inhibitor of growth reaction. Since the total amount of the solution is fixed, the pH decreases.

5.1.2 Precursor Concentration

By taking condition No.2, 6 and 7 together, the effect of precursor concentration can be shown. Figure 5.2 shows the TiO_2 nanowire substrate under different precursor concentration.

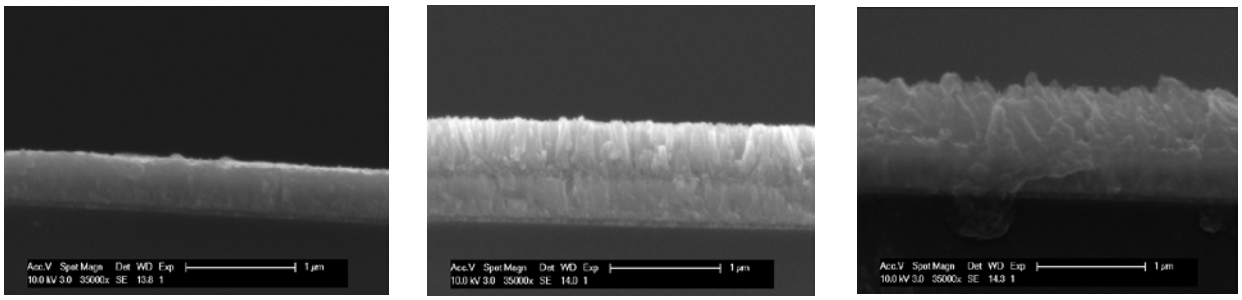

(a) (b) (c)

Figure 5.2. The effect of precursor concentration on TiO_2 nanowire length: (a) condition No.6: 1.0ml TTIP; (b) condition No.2: 1.7ml TTIP; (c) condition No.7: 2.0ml TTIP

Under low precursor concentration, HCl inhibits the nucleation and growth reaction. Thus, only a small amount of nuclei found on the FTO substrate and no nanowire found. At higher concentration, however, the concentration of nuclei is too high and causes the density of nanowire on the substrate is too high. In order to compensate this high density, the nanowires grew in a certain angle [26] instead of straight up. This makes nanowire run into neighboring nanowire and the growth stopped. As a result, the nanowire length (~550 nm) in condition No.8 is not so much higher than condition No.2 (~400nm).

5.1.3 Growth Time

By taking condition No.1, 2 and 3 together, the effect of growth time can be shown. Figure 5.3 shows the TiO_2 nanowire substrate under different growth time.

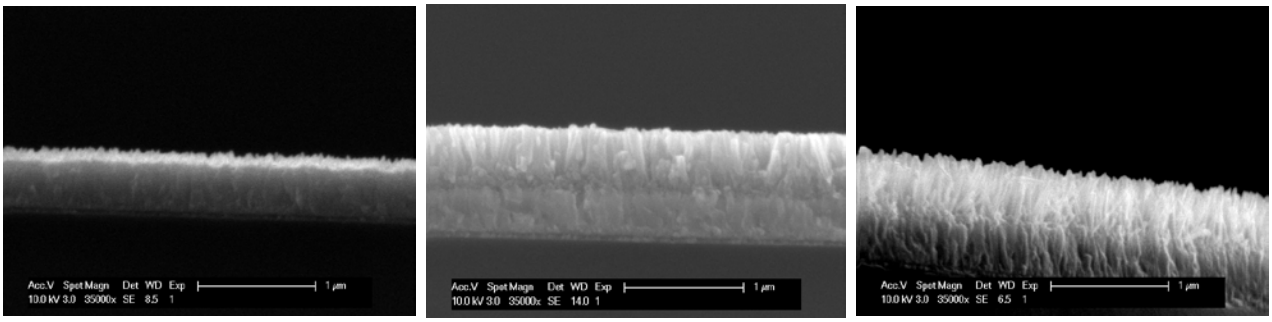

(a) (b) (c)

Figure 5.3. The effect of growth time on TiO_2 nanowire length: (a) condition No.1: 15min; (b) condition No.2: 30min; (c) condition No.3: 45min

The length of TiO_2 nanowires increases as time increases. At condition No.1 (figure 5.3(a)) the nanowires just started to grow and the length is around 100nm. Since the aspect ratio is too low,

they cannot be seen as ‘nanowire’. At condition No.2, as mention previously, the length is around 350nm. At condition No.3, the length is around 500nm. So the nanowire length in principle increases linearly with time in this time range under this concentration and temperature condition.

5.1.4 Growth Temperature

By taking condition No.2, 4 and 5 together, the effect of parameter of growth temperature can be shown. Figure 5.4 shows the TiO_2 nanowire substrate under different growth temperature.

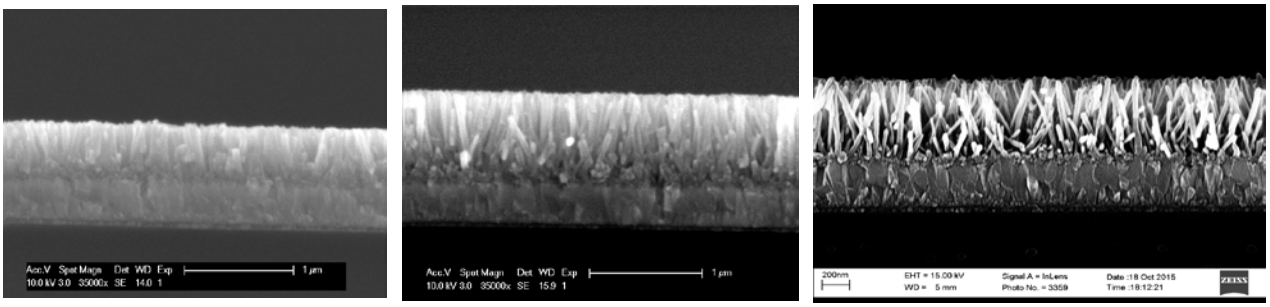

(a) (b) (c)

Figure 5.4. The effect of growth temperature on TiO_2 nanowire length: (a) condition No.2: 160℃; (b) condition No.4: 180℃; (c) condition No.5: 190℃

As shown in figure 5.4, the higher the temperature, the longer the nanowire length. The length under 160℃ is around 350 nm. Under 180℃ is around 450 nm and under 190℃ is around 600 nm. The growth increases in principle as a factor of 5. [26] No peeling effect is observed on these substrates, which means the chemical reaction does not reach equilibrium during the growth.

All the TiO_2 nanowire substrates that have length between 200-600 nm are used to fabricate NW based PSC. The NW based PSC sample that has best properties and similar thickness of TiO_2/perovskite hybrid layer as NP based PSC was used for photovoltaic measurement and make comparison in this experiment.

5.2 STATIC PHOTOVOLTAIC MEASUREMENT

5.2.1 J-V Curve

The J-V curves of high quality TiO_2 NP based and TiO_2 NW based perovskite solar cell are shown in figure 5.5.

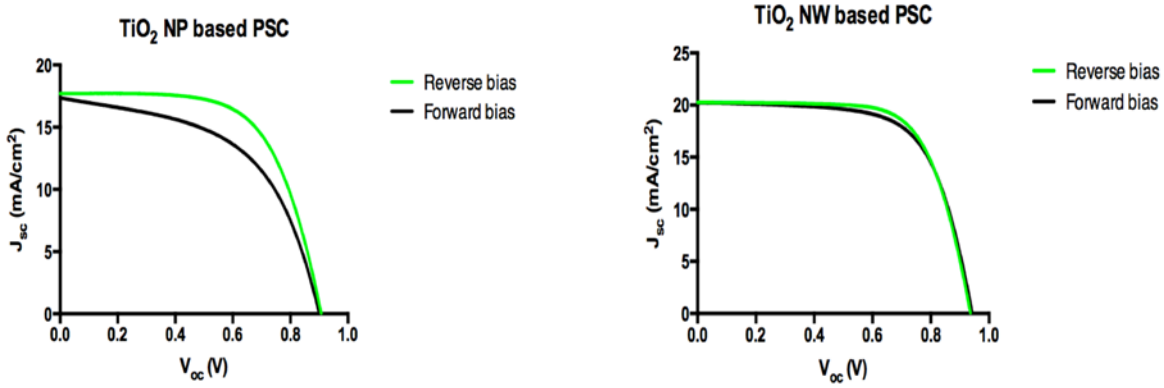

(a) (b)

Figure 5.5. The J-V curve of PSC sample: (a) TiO_2 NP based PSC; (b) TiO_2 NP based PSC

The data, including J_{sc}, V_{oc}, PCE and fill factor (FF), of the J-V curves in listed below in table 5.1.

Table 5.1. Data from I-V curve

Sample	J_{sc} (mA/cm^2)	V_{oc} (V)	PCE (%)	FF
TiO_2 NP (Reverse bias)	17.7	0.907	10.2	0.635
TiO_2 NP (Forward bias)	17.3	0.900	8.26	0.529
TiO_2 NW (Reverse bias)	20.3	0.936	13.0	0.687
TiO_2 NW (Forward bias)	20.2	0.942	12.6	0.661

Figure 5.5 and Table 5.1 show the overall PCE of NP and NW based PSC are similar, the TiO_2 NP based PSC has higher V_{oc} compared to TiO_2 NW based PSC. On the other hand, the J_{sc} and FF of TiO_2 NW based PSC are higher than those TiO_2 NP based PSC.

J-V curves in Figure 5.5 are measured by forward bias and reverse bias scans. The reverse scans in both NP based samples and NW based sample provided better performance compared to the forward scans. Though there was not much change in photocurrent and voltage, fill factor decreased dramatically in the forward scans. The efficiency in reverse scan does not change much when the thickness of TiO_2 mesoporous layer. However, the forward scans yielded obviously. This behavior of hysteresis that efficiency depend on scan direction is because charges need redistribution and reaches a new equilibrium state, which may be related to the large diffusion capacitance of the perovskite solar cell. [47], [48]

5.2.2 Microstructure Comparison

SEM was used to obtain the images of nanostructures of TiO_2 NP and NW based substrate, which are shown in Figure 5.6.

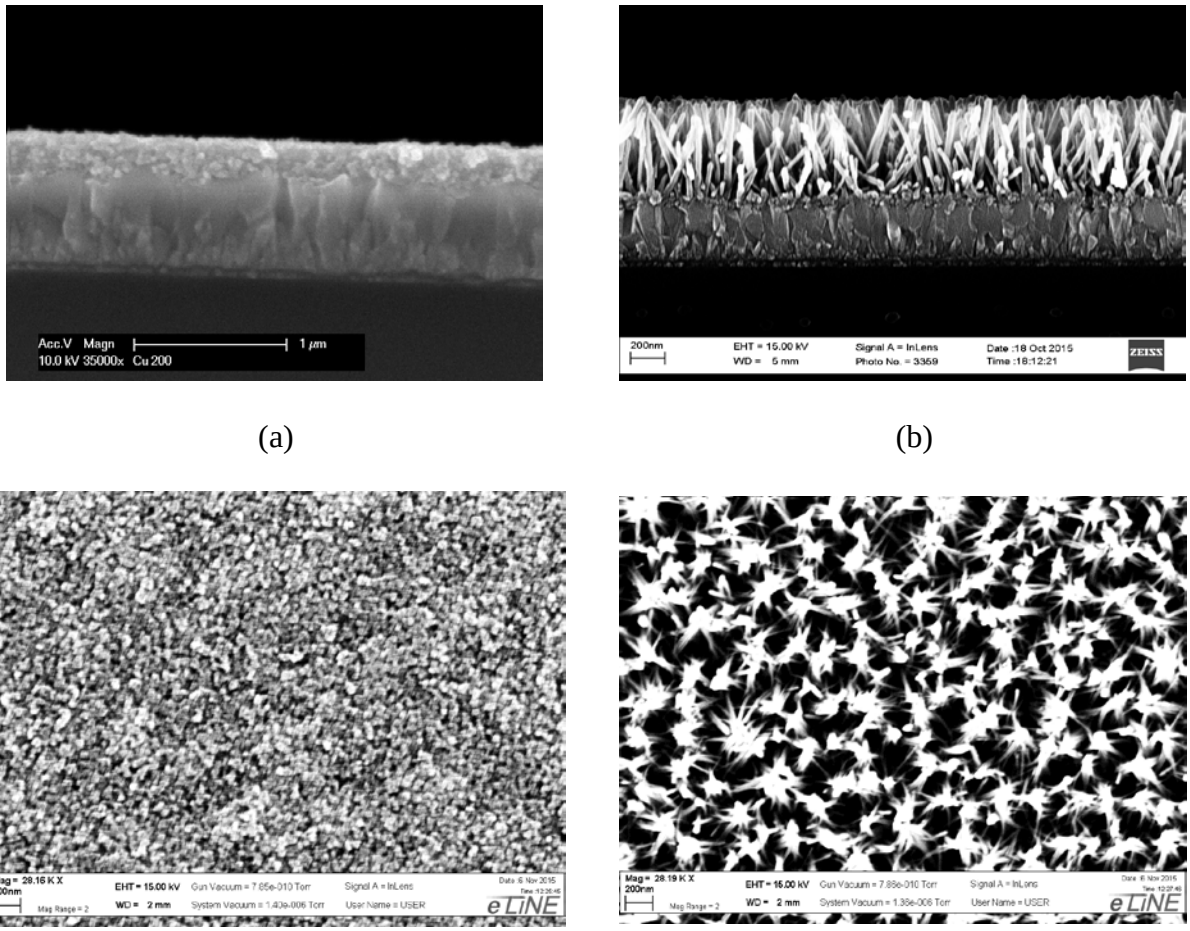

Figure 5.6. The SEM images of TiO_2 NP and NW substrate: (a) NP based cross-section; (b) NW based cross-section; (c) NP based top view; (d) NW based top view

These SEM images were taken from the TiO_2 deposited substrates that have the same fabrication condition as the solar cells that produced the J-V curve in Figure 5.5. The thickness of TiO_2 nanoparticle is around 200 nm. The PCE, V_{oc} and FF of the perovskite solar cell will decrease if the thickness of TiO_2 nanoparticle layer further increases, because the length of electron diffusion and chance of recombination increase. In the TiO_2 nanowire substrate, the length of nanowire is around 600nm, which is far higher than nanoparticle layer in Figure 5.6(a),

and aspect ratio is around 15. Figure 5.7 shows the cross-section nanostructure of perovskite solar cell.

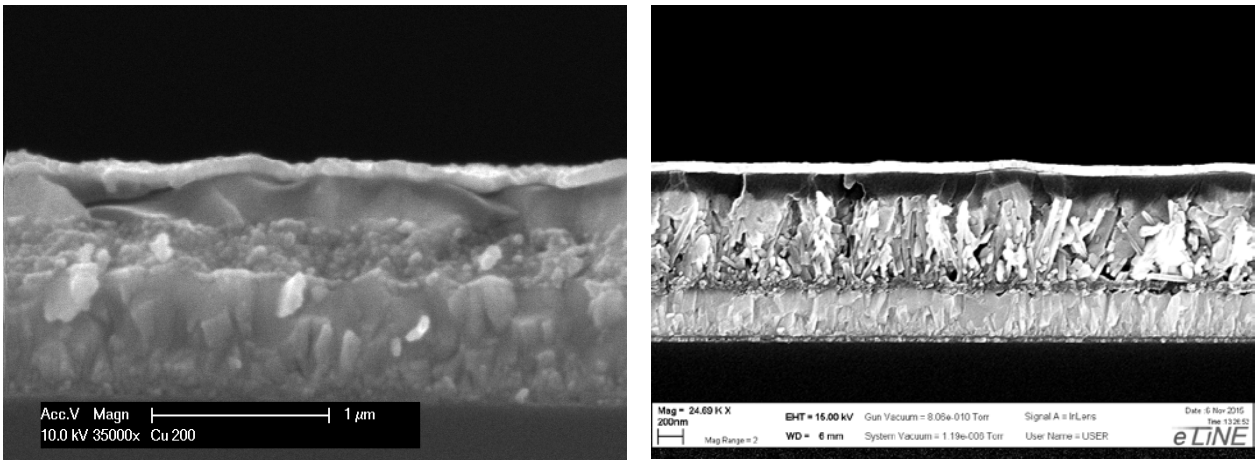

(a) (b)

Figure 5.7. The SEM images of TiO_2 NP and NW based PSC (a) NP based PSC; (b) NW based PSC

The total thickness of TiO_2 nanoparticle/perovskite layer in figure 5.7(a) is around 500 nm, where TiO_2 nanoparticle layer is only 200 nm thick. The 300 nm thick perovskite layer refers to the cuboid structure. [34] The crystal size of cuboid crystal is in a negative relationship with the concentration of MAI solution, which is 7 mg/mL (0.044 M) in this experiment. In principle, 0.044 M MAI solutions can produce perovskite crystal with grain size around 300 nm. [34] The hysteresis of I-V curve scanning direction is also related to the size of cuboid crystal. When the cuboid is produced by low concentration MAI, the dependency can be ignored. On the contrary, the dependency is significant. [34] Besides, crystalline perovskite infiltrates the mesoporous TiO_2 and results in miscellaneous order of perovskite and TiO_2 in the light absorber layer. Figure 5.7(b) shows no explicit perovskite cuboid layer occurs on top of TiO_2 nanowire

structure. The thickness of TiO_2/perovskite is around 600 nm, which is similar to the thickness in nanoparticle based PSC sample. TiO_2 nanowire and perovskite are well aligned in the light absorber layer. In TiO_2 nanoparticle based PSC, the HTM layer infiltrated in the interspace of perovskite cuboid crystal grains, while in TiO_2 nanowire based PSC, the HTM layer (dark) is explicit located on the top of TiO_2/perovskite layer. In addition, the thin layer on the top of the samples is Au electrode.

5.2.3 UV/Vis Spectroscopy

To figure out how many photons absorbed by perovskite solar cell, both NP and NW based perovskite solar cell along with their FTO substrates and TiO_2 deposited substrates were measure under UV/Vis spectroscopies.

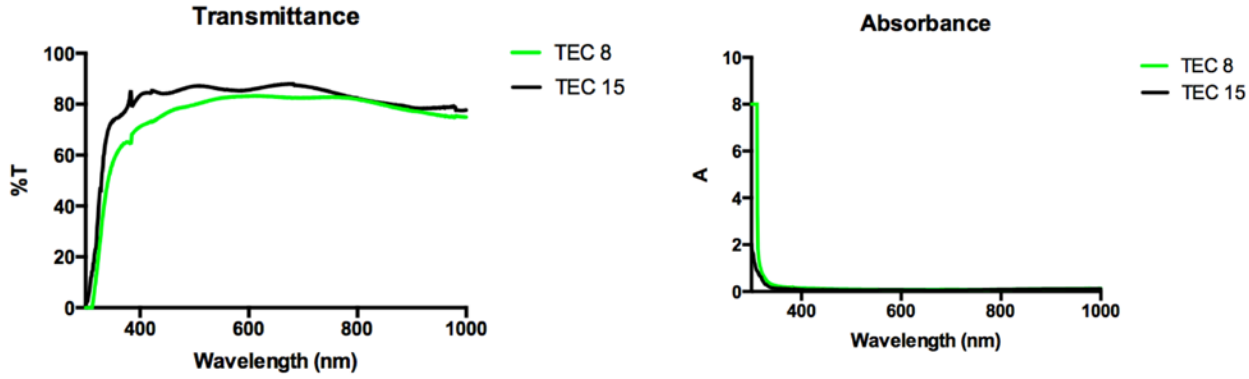

(a) (b)

Figure 5.8. The UV/Vis figure of 2 kinds of FTO glass: (a) Transmittance; (b) Absorbance

It is obviously that TEC8 FTO substrate, which used in TiO_2 NP based PSC has lower transmittance compared to TEC15 FTO that used in in TiO_2 NW based PSC. The transmittance

curves of both TEC8 and TEC15 kept almost constant in wavelength range of 400-1000 nm but dramatic decreased in the range of 300-400 nm, which is the UV zone. Meanwhile, the absorbance curve increased dramatically in this range.

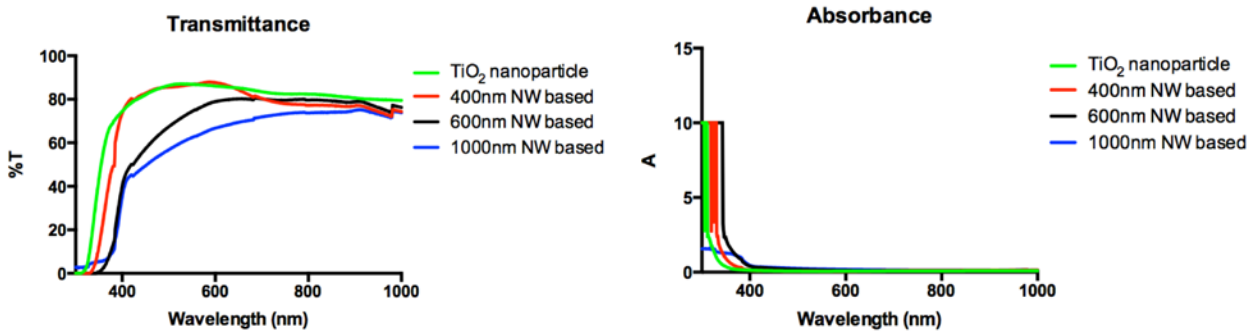

(a) (b)

Figure 5.9. The UV/Vis figure of 2 kinds of TiO_2 deposited glass substrates: (a) Transmittance; (b) Absorbance

Though pure TEC8 FTO has lower transmittance, after TiO_2 deposition, the NP substrate had even higher transmittance as NW substrates. From experimental point of view, after TiO_2 nanowire growth, the substrates looked vague while nanoparticle substrates still kept transparent.

The transmittance of TiO_2 nanowire sample is a function of nanowire length. The transmittance decreases remarkably as the nanowire length increases. The absorbance curves showed the opposite behavior as transmittance curves.

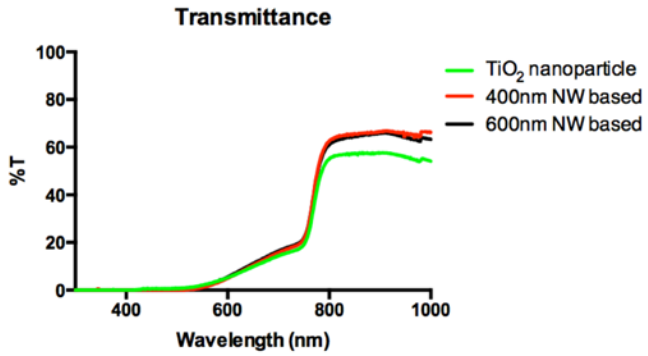

Figure 5.10. The UV/Vis transmittance figure of TiO_2 perovskite solar cell

Since the nanowire substrate with 1000 nm in length does not fit the requirement, only the nanowire samples with 400 nm and 600 nm in length were used for solar cell fabrication. In Figure 5.10, the nanoparticle based perovskite solar cell sample has lowest transmittance and 400 nm NW based perovskite solar cell sample has the highest transparency. Though in the wavelength range of 800-1000 nm, NW based PSC has higher transmittance, they all have almost same transmittance in the range of 300-800 nm, which counts most in IPCE measurement.

5.2.4 DC Mode IPCE

The DC mode IPCE measurement was made on NP and NW based PSC and the IPCE curves are shown below in Figure 5.11.

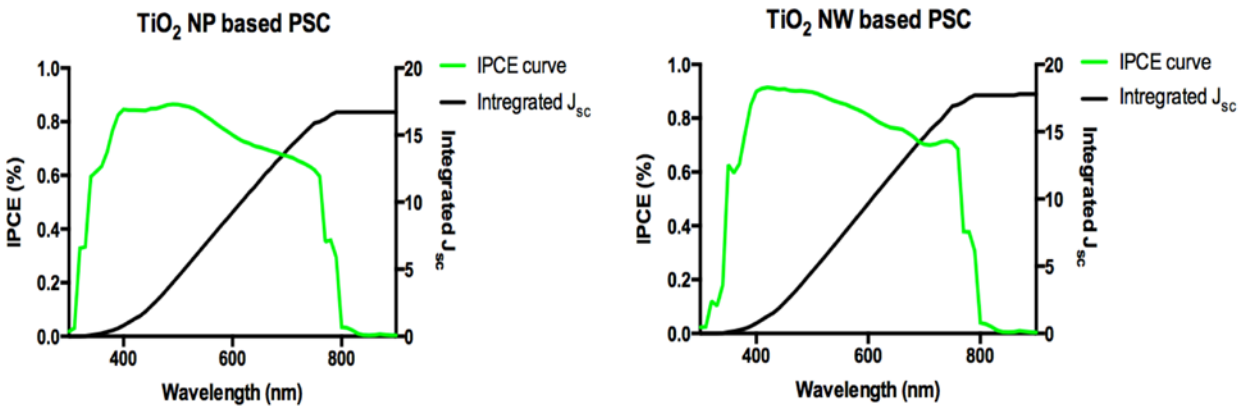

(a) (b)

Figure 5.11. The DC mode IPCE curves of PSC sample: (a) TiO_2 NP based PSC; (b) TiO_2 NP based PSC

Though Figure 5.11 (a) and (b) show slightly different in the data value, the curve's shape are mostly the same, which indicates the DC mode IPCE of TiO_2 NP based PSC are similar to TiO_2 NW based PSC. The maximum IPCE value in TiO_2 NP based PSC exceeds 80% and exceeds 90% in TiO_2 NW based PSC. The decrease in the range of 570-750 nm results in a narrow plateau that over 80% and the integral J_{sc} value decrease. The J_{sc} curve is integrated from the IPCE curve as a function of wavelength. As a result, nanowire based sample has higher J_{sc} compared to nanoparticle based sample.

5.3 DYNAMIC PHOTOVOLTAIC MEASUREMENT

5.3.1 AC Mode IPCE

Figure 5.12 shows the AC mode IPCE of TiO_2 nanoparticle based perovskite solar cell. The frequencies of the shutter that have been tested are 1Hz, 10Hz, 30Hz, 50Hz, 75Hz and 95Hz. Meanwhile, DC mode IPCE curve is also added as the condition of 0Hz.

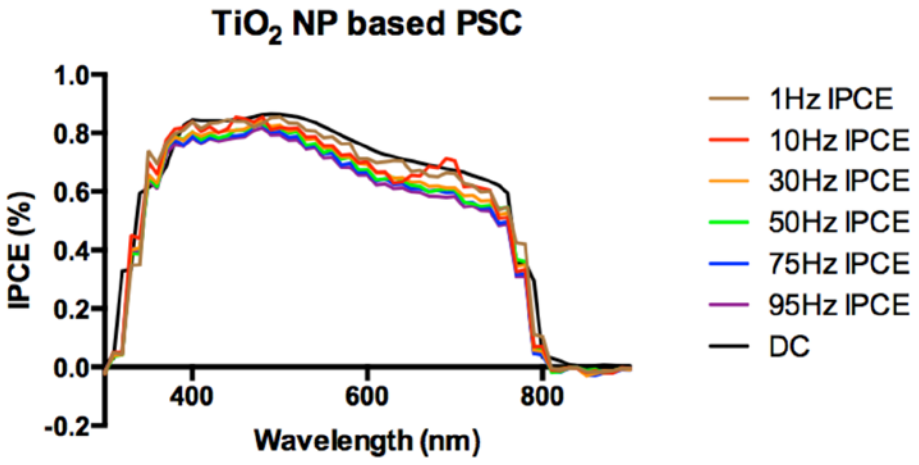

Figure 5.12. The AC mode IPCE curves of TiO_2 nanoparticle based PSC sample

Figure 5.13 shows the AC mode IPCE of TiO_2 nanoparticle based perovskite solar cell.

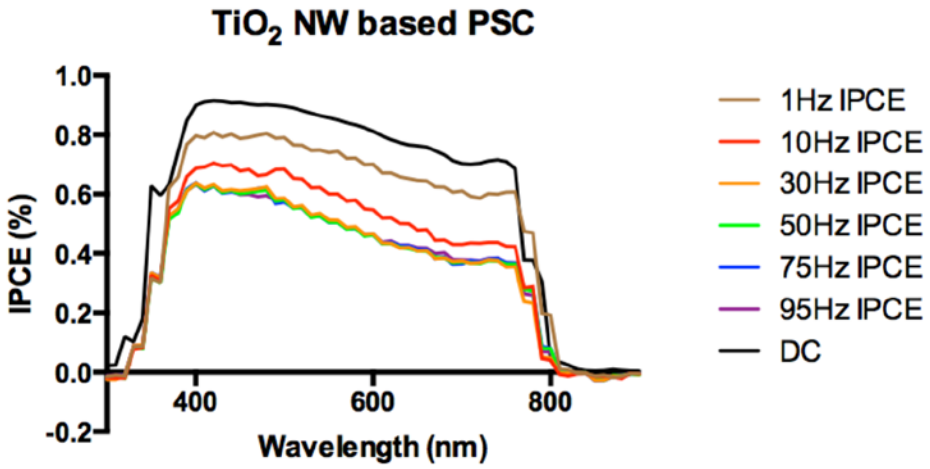

Figure 5.13. The AC mode IPCE curves of TiO_2 nanowire based PSC sample

Figure 5.12 shows a gradual decrease of IPCE in TiO_2 NP based PSC as the illumination frequency increases. In Figure 5.13, the decrease of TiO_2 NW based PSC is severer in the frequency range of 0 Hz to 10 Hz compared to NP based solar cell. However, as the illumination frequency is higher than 30 Hz, a change in IPCE is saturated and spectra overlap.

In DC mode IPCE, the solar cell sample ia exposed to steady-state illumination and electrons fulfilled the traps, which are caused by defects in the crystal lattice. As a result, the DC mode IPCE does not depend on the concentration of traps. However, in AC mode IPCE, electrons are trapped during diffusion and extraction.

Except DC and 1Hz, all other studied frequencies are high enough and photocurrents do not reaching their steady-state value, which results in slow response. The trapped electrons cannot be fully released due to the short time interval. Thus, the peak-to-peak values of photocurrent become lower, which make the AC mode IPCE spectra depended on the trap state capacitance significantly. As a result, IPCE curve drops as frequency increase, no matter how much dependence is on frequency. [49], [53]

5.3.2 Carrier Lifetime Measurement

Results from carrier life measurement are shown in figure 5.14 below. SLIM-PCV measurement is used to obtain diffusion coefficient from photocurrent decay and electron lifetime from voltage decay. The thickness in TiO_2 nanoparticle based PSC sample is 500nm and TiO_2 nanowire based PSC is 600nm as shown in Figure 5.7.

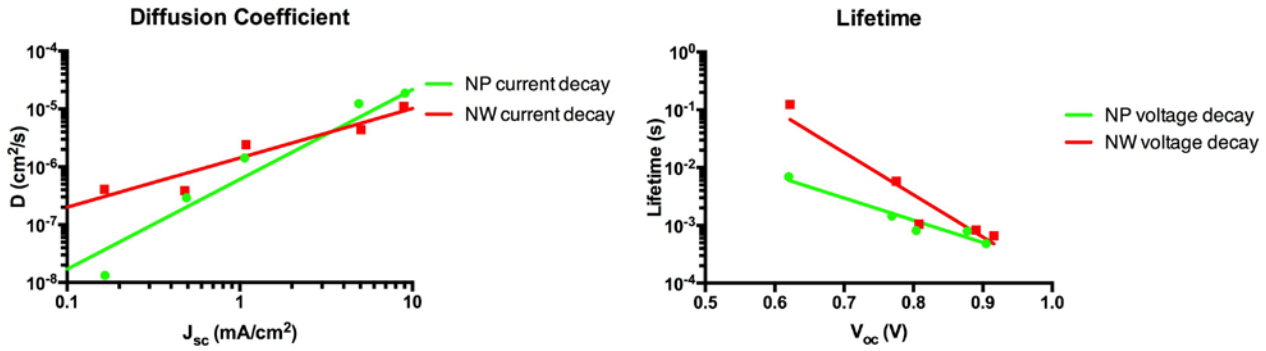

(a) (b)

Figure 5.14. Carrier lifetime measurement: (a) Photocurrent decay; (b) Voltage decay

Both J_{sc} and V_{oc} decay as light intensity decays. So data points at high J_{sc} and V_{oc} are measured under high light intensities. In Figure 5.14(a), at lower J_{sc}, TiO_2 nanowire based PSC has higher diffusion coefficient. However, TiO_2 nanoparticle based PSC has similar diffusion coefficient as nanowire based sample. The reason for high diffusion coefficient in nanowire-based sample is the single crystalline nanowire has less trapping sites, which can improve the diffusivity. [21]

In Figure 5.14(b), TiO_2 rutile single crystalline nanowire has fast electron transportation rate and less trapping sites, so it has low recombination rate when light intensity and V_{oc} are low.

Thus, NW based PSC has longer electron lifetime compared to NP based PSC. However, when light intensity and V_{oc} are high, the lifetime in NW based PSC is suppressed more than NP based PSC.

5.4 DISCUSSION

In static photovoltaic measurements, TiO_2 nanoparticle and nanowire based PSCs showed similar results. Slight difference appeared in I-V curve and DC mode IPCE. The carrier diffusion coefficient and concentration of traps in nanowire based PSCs are lower, so that they have higher V_{oc}. Since TiO_2 nanowire based PSCs have lower number of defects and traps, they have higher fill factors compared to nanoparticle based PSCs. Besides, nanoparticle based PSC samples show high hysteresis behavior from I-V curve, especially in the voltage range of 0.3-0.7 V, which means electrons' diffusion under this voltage range is much harder than TiO_2 nanowire based PSCs.

In dynamic photovoltaic measurements, TiO_2 nanoparticle based PSCs show gradual change in data measured under different conditions, both in AC mode IPCE and carrier lifetime measurement. Though TiO_2 nanowire based PSCs have better properties related to carrier transportation, they show bigger changes in dynamic photovoltaic measurement. As a result, a reason that helps carrier transporting in TiO_2 nanowire based PSCs is suppressed by frequency and high light intensity.

Space charge polarization is a behavior that appears commonly in PSC, especially TiO_2 nanowire based PSC. The formation of space charge polarization can help carrier transport under electric field. Photogenerated charges can be accumulated at the interfacial area where bulk

defects appear. [54] This surface charge accumulation forms an internal electric field that impedes electron extraction. Space charges dipoles, however, has a direction opposite to internal electric field, which enhance electron extraction. Figure 5.15 shows the space charge polarization behavior in TiO_2 nanoparticle based PSCs, where red dots stand for holes and blue dots stand for electrons. Black region is perovskite and white region is TiO_2. The dipoles in nanoparticle structure are miscellaneous distributed and thus the space charge polarization is not so powerful that can support electron extraction effectively.

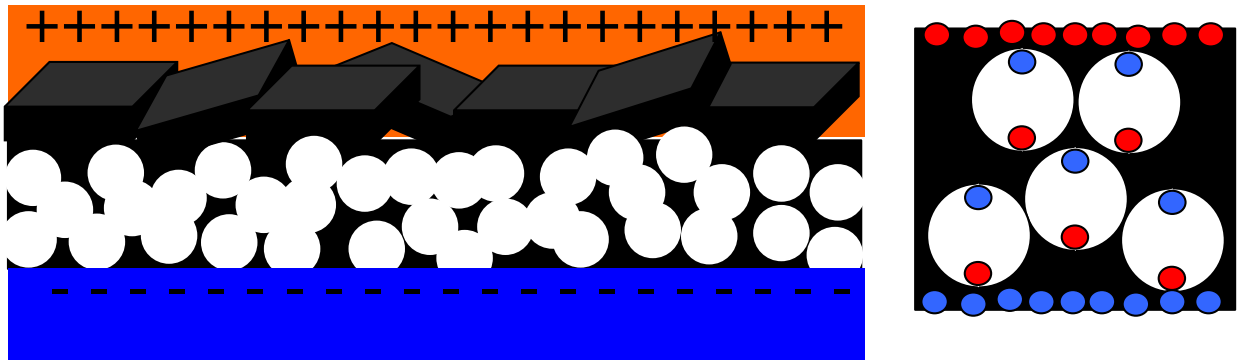

(a) (b)

Figure 5.15. Schematic of space charge polarization in TiO_2 nanoparticle based PSC: (a) TiO2 nanoparticle based PSC cross-section; (b) Space charge polarization illustration

However, in TiO_2 nanowire based perovskite solar cell, as shown in figure 5.16, the dipoles are well aligned. Electron generated in perovskite transport into TiO_2 nanowire and eventually into n-type contact under the electric field formed by dipoles in TiO_2 nanowire. The well-aligned dipoles produce a strong space charge polarization field and eventually make the electron extraction more efficient.

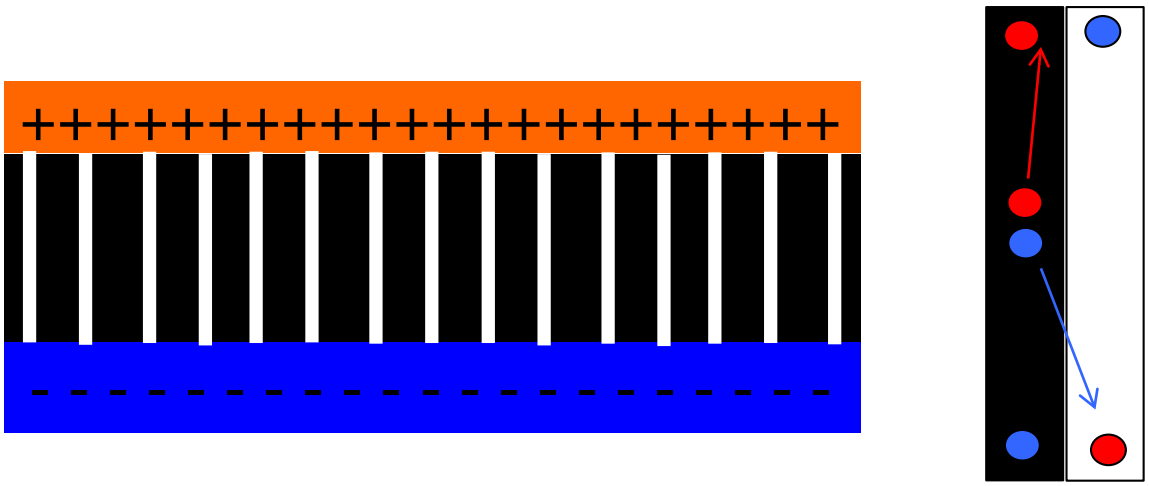

(a) (b)

Figure 5.16. Schematic of space charge polarization in TiO_2 nanowire based PSC: (a) TiO2 nanowire based PSC cross-section; (b) Space charge polarization illustration

When frequency added in IPCE, the photocurrents in TiO_2 nanowire based perovskite solar cells are suppressed seriously, however, only slight decrease in nanoparticle based PSCs occur. The reason is due to the lengths of nanowire are much longer than the radii of nanoparticle, so that it takes much longer time for TiO_2 nanowire based PSCs to fully build up the space charge polarization field. In AC mode IPCE, the expose time is too short for building up effective well-aligned polarization field. Besides, a remarkable ratio of electrons is depleted when the chopper blocks the light. TiO_2 nanoparticle based PSCs, on the contrary, have enough time to build up space charge polarization in TiO_2 nanoparticles even when the expose time is limited. Though the effect of polarization is less powerful as the one in nanowire based PSCs under steady state, it can still enhance electron extraction under high frequency.

Figure 5.17 below shows how surface charge accumulation and space charge polarization affect the charge distribution in perovskite light absorber layer.

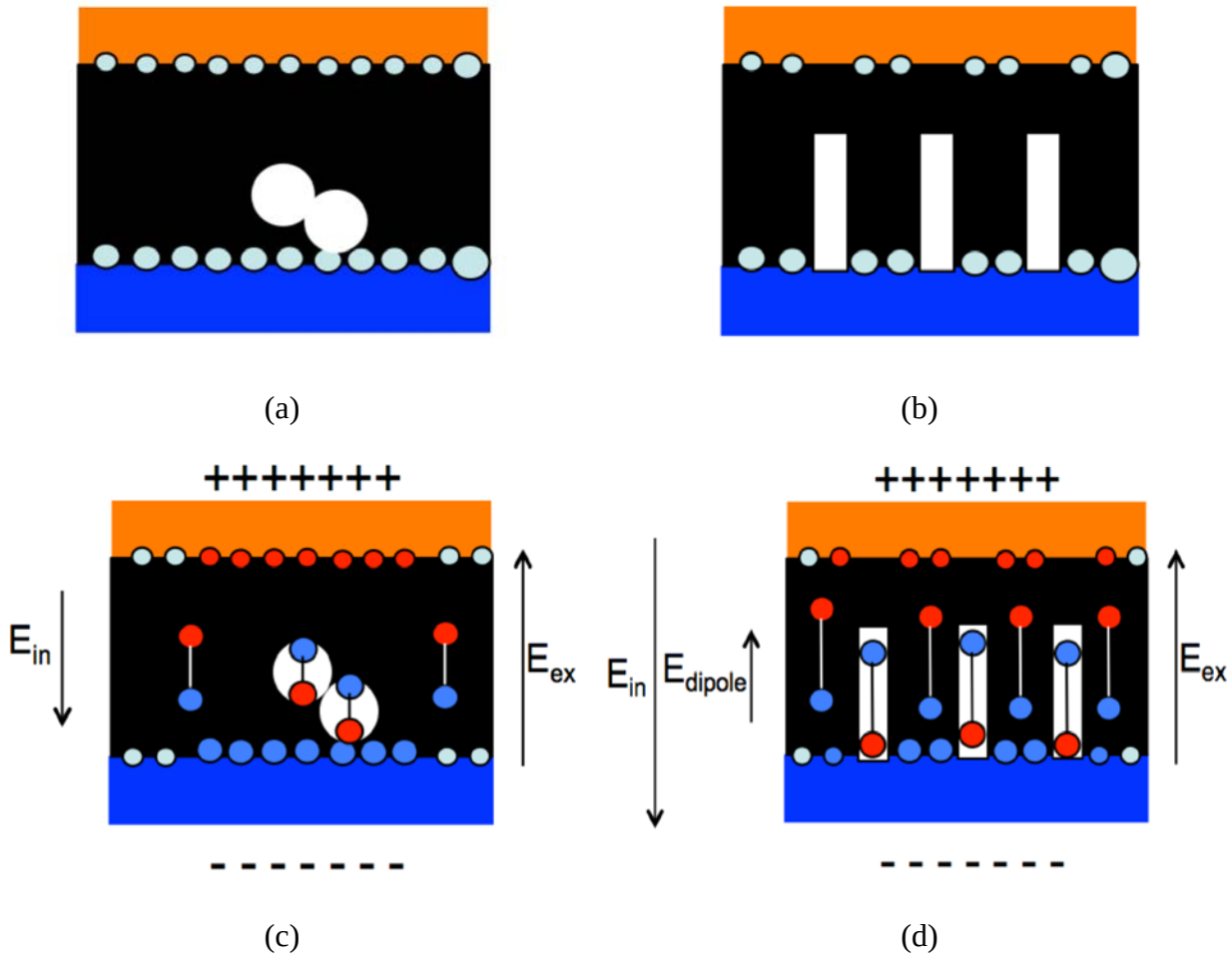

Figure 5.17. Schematic of PSCs: (a) TiO_2 nanoparticle based under SC condition; (b): TiO_2 nanowire based under SC condition (c) TiO_2 nanoparticle based under FB condition; (d) TiO_2 nanowire based under FB condition

In figure 5.17, gray dots stand for empty surface defects. SC stand for short-circuit condition and FB stand for forward bias condition. In reverse scan, the I-V curves are produced from FB condition to SC condition, which means external bias decreases as scan processing. On the contrary, they are produced from SC to FB in forward scan and external bias increases as scan processing. Because TiO_2 nanoparticle based PSC samples have more serious hysteresis behavior, in forward scan, as external bias increasing, more carriers are trapped at surface defects

in TiO_2 nanoparticle based PSCs than those in nanowire based PSCs. This is the direct reason for hysteresis behavior.

This direct reason can be caused by many further reasons. The hysteresis is related to large defect density in the interface of light absorber layer and n- or p- type contact. [57] Besides, the large cuboid crystal size is another issue of hysteresis in nanoparticle based PSC. [56] Since TiO_2 nanoparticle based PSCs have more defects near the material surface, which play a role as traps for carriers. These traps are filled under forward bias. However, under short-circuit conditions, they may become empty because charges transfer to n-type and p-type layer at the interfaces. This causes the hysteresis in forward scan since charge refilling time for traps is required. [57] According to Figure 5.14, the diffusion coefficient in TiO_2 nanoparticle based PSC is low, which causes slow dynamic in perovskite absorber layer, so that the charge emptying and filling rate are low. TiO_2 nanowire based PSC samples, on the contrary, has high diffusion coefficient. Space charge effect shown in figure 5.15 also helps the diffusion of electrons. As a result, the hysteresis behavior is less in nanowire based PSCs.

Besides the slow dynamic and high surface defect concentration, less effective space charge polarization effect caused many miscellaneous dipoles is also a part of reason for hysteresis. Under short circuit condition, the surface defects at interface are vacant in both nanoparticle and nanowire based PSC, thus no dipoles formed in the light absorber layer. When positive bias applied, as shown in Figure 5.17(d), the well-aligned dipoles in TiO_2 nanowire enhance the electron extraction effectively by compensating the internal electric field formed by surface charge accumulation. In TiO_2 nanoparticle based PSCs this compensating is not powerful, so the electron extraction is impeded seriously by the surface charge accumulation. As a result,

the difficulty of carrier transportation is high in nanoparticle based PSCs when positive bias is applied and hysteresis become large.

6.0 CONCLUSION

This thesis topic is related to TiO_2 based perovskite solar cell. Two morphology types of perovskite solar cells are fabricated and carrier-transporting behaviors have been studied. Space charge polarization effect is studied in order to explain the differences in carrier transportation of TiO_2 nanoparticle and nanowire based perovskite solar cell.

TiO_2 nanowire substrates were fabricated under different parameters. This fabrication is very sensitive. As a result, it takes time to fix the condition of fabrication. Similar properties of two morphology types of perovskite solar cells have been displayed by static photovoltaic measurements. I-V measurement shows significant hysteresis behavior in TiO_2 nanoparticle based perovskite solar cell. AC mode IPCE measurement shows the high frequency dependence in TiO_2 nanowire based perovskite solar cell. Carrier lifetime measurement displays the diffusion coefficient and carrier lifetime as a function of light intensity.

Two major behaviors are discussed in perovskite solar cell: hysteresis and frequency dependence. The hysteresis behavior is caused by large ratio of carriers trapped by surface defects and accumulated to form an internal electric field that impedes carrier extraction. High density of surface defects, low charge diffusion coefficient, which correspond to the results from carrier lifetime measurement, and miscellaneous space charge dipoles are the reason for high hysteresis in TiO_2 nanoparticle based PSCs. The reason for high frequency dependence in TiO_2 nanowire based PSCs is space charge polarization effect is suppressed when the frequency is

applied due to the long time required for building up the polarization. Though TiO_2 nanoparticle based PSCs have powerless space charge polarization effect, the light exposure time is sufficient for building polarization up. As a result, TiO_2 nanowire based PSCs decrease dramatically in IPCE when frequency applied and TiO_2 nanoparticle based PSCs only behave as slight decreases.

BIBLIOGRAPHY

[1] "Industry Market Trends." Is Perovskite the Future of Solar Cells? N.p., 06 Dec. 2013. Web. 21 Jan. 2015.

[2] Neamen, Donald A. Semiconductor physics and devices. McGraw-Hill Higher Education, 2003.

[3] Snaith, Henry J. "Perovskites: The Emergence of a New Era for Low-Cost, High-Efficiency Solar Cells." The Journal of Physical Chemistry Letters4.21 (2013): 3623-630. Web.

[4] Chen, Qi, Huanping Zhou, Ziruo Hong, Song Luo, Hsin-Sheng Duan, Hsin-Hua Wang, Yongsheng Liu, Gang Li, and Yang Yang. "Planar Heterojunction Perovskite Solar Cells via Vapor-Assisted Solution Process." Journal of the American Chemical Society 136.2 (2014): 622-25. Web.

[5] Carlson, D., Wronski, C. (1985). Topics in Applied Physics: Amorphous Semiconductors: Amorphous silicon solar cells. Springer Berlin / Heidelberg.

[6] Dalven, R., and Nicolaas Bloembergen. "Introduction to Applied Solid State Physics: Topics in the Applications of Semiconductors, Superconductors, and the Nonlinear Optical Properties of Solids." Physics Today 33.9 (2008): 69-70.

[7] Kasap, Safa O. Principles of electronic materials and devices. Vol. 81. New York, NY: McGraw-Hill, 2006.

[8] Kojima, Akihiro; Teshima, Kenjiro; Shirai, Yasuo; Miyasaka, Tsutomu (6 May 2009). "Organometal Halide Perovskites as Visible-Light Sensitizers for Photovoltaic Cells". Journal of the American Chemical Society 131 (17): 6050–6051. doi:10.1021/ja809598r. PMID 19366264

[9] Im, Jeong-Hyeok; Lee, Chang-Ryul; Lee, Jin-Wook; Park, Sang-Won; Park, Nam-Gyu (2011). "6.5% efficient perovskite quantum-dot-sensitized solar cell". Nanoscale 3 (10): 4088. doi:10.1039/C1NR10867K.

[10] Lee, M. M.; Teuscher, J.; Miyasaka, T.; Murakami, T. N.; Snaith, H. J. (4 October 2012). "Efficient Hybrid Solar Cells Based on Meso-Superstructured Organometal Halide Perovskites". Science 338 (6107): 643–647. doi:10.1126/science.1228604.

[11] Kim, Hui-Seon; Lee, Chang-Ryul; Im, Jeong-Hyeok; Lee, Ki-Beom; Moehl, Thomas; Marchioro, Arianna; Moon, Soo-Jin; Humphry-Baker, Robin; Yum, Jun-Ho; Moser, Jacques E.; Grätzel, Michael; Park, Nam-Gyu (21 August 2012). "Lead Iodide Perovskite Sensitized All-Solid-State Submicron Thin Film Mesoscopic Solar Cell with Efficiency Exceeding 9%". Scientific Reports 2. doi:10.1038/srep00591

[12] Liu, Mingzhen, Michael B. Johnston, and Henry J. Snaith. "Efficient Planar Heterojunction Perovskite Solar Cells by Vapour Deposition." Nature501.7467 (2013): 395-98. Web.

[13] Burschka, Julian; Pellet, Norman; Moon, Soo-Jin; Humphry-Baker, Robin; Gao, Peng; Nazeeruddin, Mohammad K.; Grätzel, Michael (10 July 2013). "Sequential deposition as a route to high-performance perovskite-sensitized solar cells". Nature 499 (7458): 316–319. doi:10.1038/nature12340.

[14] Liu, Mingzhen; Johnston, Michael B.; Snaith, Henry J. (11 September 2013). "Efficient planar heterojunction perovskite solar cells by vapour deposition". Nature 501 (7467): 395–398. doi:10.1038/nature12509.

[15] Docampo, Pablo; Ball, James M.; Darwich, Mariam; Eperon, Giles E.; Snaith, Henry J. (12 November 2013). "Efficient organometal trihalide perovskite planar-heterojunction solar cells on flexible polymer substrates". Nature Communications 4. doi:10.1038/ncomms3761

[16] Zhou, H.; Chen, Q.; Li, G.; Luo, S.; Song, T.-b.; Duan, H.-S.; Hong, Z.; You, J.; Liu, Y.; Yang, Y. (31 July 2014). "Interface engineering of highly efficient perovskite solar cells". Science 345 (6196): 542–546. doi:10.1126/science.1254050

[17] Im, Jeong-Hyeok, et al. "Nanowire Perovskite Solar Cell." Nano letters 15.3 (2015): 2120-2126.

[18] Liu, Jian, et al. "A dopant-free hole-transporting material for efficient and stable perovskite solar cells." Energy & Environmental Science 7.9 (2014): 2963-2967.

[19] Leijtens, Tomas, et al. "Overcoming ultraviolet light instability of sensitized TiO2 with meso-superstructured organometal tri-halide perovskite solar cells." Nature communications 4 (2013).

[20] Kasap, Safa O. Principles of electronic materials and devices. McGraw-Hill, 2006.

[21] Yang, Mengjin, et al. "Carrier transport in dye-sensitized solar cells using single crystalline TiO2 nanorods grown by a microwave-assisted hydrothermal reaction." The Journal of Physical Chemistry C 115.30 (2011): 14534-14541.

[22] Burschka, Julian, et al. "Sequential deposition as a route to high-performance perovskite-sensitized solar cells." Nature 499.7458 (2013): 316-319.

[23] Misra, Ravi K., et al. "Temperature-and Component-Dependent Degradation of Perovskite Photovoltaic Materials under Concentrated Sunlight." The Journal of Physical Chemistry Letters 6.3 (2015): 326-330.

[24] Macdonald, J. Ross. "Theory of ac space-charge polarization effects in photoconductors, semiconductors, and electrolytes." Physical review 92.1 (1953): 4.

[25] Fan, Jiandong, Baohua Jia, and Min Gu. "Perovskite-based low-cost and high-efficiency hybrid halide solar cells." Photonics Research 2.5 (2014): 111-120.

[26] Liu, Bin, and Eray S. Aydil. "Growth of oriented single-crystalline rutile TiO2 nanorods on transparent conducting substrates for dye-sensitized solar cells." Journal of the American Chemical Society 131.11 (2009): 3985-3990.

[27] Li, Yuxiang, et al. "Hydrothermal synthesis and characterization of TiO 2 nanorod arrays on glass substrates." Materials Research Bulletin 44.6 (2009): 1232-1237.

[28] Wang, Hong-En, et al. "Hydrothermal synthesis of ordered single-crystalline rutile TiO2 nanorod arrays on different substrates." Applied Physics Letters 96.26 (2010): 263104.

[29] Nian, Jun-Nan, and Hsisheng Teng. "Hydrothermal synthesis of single-crystalline anatase TiO2 nanorods with nanotubes as the precursor." The Journal of Physical Chemistry B 110.9 (2006): 4193-4198.

[30] Deng, Qixin, et al. "Selective synthesis of rutile, anatase, and brookite nanorods by a hydrothermal route." Current Nanoscience 6.5 (2010): 479-482.

[31] Bokhimi, X., et al. "Local order in titania polymorphs." International journal of hydrogen energy 26.12 (2001): 1279-1287.

[32] Hartman, Piet, and W. G. Perdok. "On the relations between structure and morphology of crystals. I." Acta Crystallographica 8.1 (1955): 49-52.

[33] Vayssieres, Lionel, et al. "Purpose-built anisotropic metal oxide material: 3D highly oriented microrod array of ZnO." The Journal of Physical Chemistry B 105.16 (2001): 3350-3352.

[34] Im, Jeong-Hyeok, et al. "Growth of CH3NH3PbI3 cuboids with controlled size for high-efficiency perovskite solar cells." Nature nanotechnology 9.11 (2014): 927-932.

[35] Kissinger, Homer E. "Reaction kinetics in differential thermal analysis." Analytical chemistry 29.11 (1957): 1702-1706.

[36] Abate, Antonio, et al. "Lithium salts as “redox active” p-type dopants for organic semiconductors and their impact in solid-state dye-sensitized solar cells." Physical Chemistry Chemical Physics 15.7 (2013): 2572-2579.

[37] "The Multispectral Sun, from the National Earth Science Teachers Association". Windows2universe.org. 2007-04-18. Retrieved 2012-02-12.

[38] Kayes, Brendan M., et al. "27.6% Conversion efficiency, a new record for single-junction solar cells under 1 sun illumination." Photovoltaic Specialists Conference (PVSC), 2011 37th IEEE. IEEE, 2011.

[39] Mills, George D. "Ultraviolet/Visible Spectroscopy." (2012).

[40] Mahan, John E. "Physical vapor deposition of thin films." Physical Vapor Deposition of Thin Films, by John E. Mahan, pp. 336. ISBN 0-471-33001-9. Wiley-VCH, January 2000. 1 (2000).

[41] O'Regan, Brian C., et al. "Influence of the TiCl4 treatment on nanocrystalline TiO2 films in dye-sensitized solar cells. 2. Charge density, band edge shifts, and quantification of recombination losses at short circuit." The Journal of Physical Chemistry C 111.37 (2007): 14001-14010.

[42] Kojima, Akihiro, et al. "Organometal halide perovskites as visible-light sensitizers for photovoltaic cells." Journal of the American Chemical Society 131.17 (2009): 6050-6051.

[43] Kim, Hui-Seon, et al. "High efficiency solid-state sensitized solar cell-based on submicrometer rutile TiO2 nanorod and CH3NH3PbI3 perovskite sensitizer." Nano letters 13.6 (2013): 2412-2417.

[44] Eperon, Giles E., et al. "Morphological Control for High Performance, Solution-Processed Planar Heterojunction Perovskite Solar Cells." Advanced Functional Materials 24.1 (2014): 151-157.

[45] Greenwood, Norman Neill, and Alan Earnshaw. "Chemistry of the Elements." (1984).

[46] Van Slyke, S. A., C. H. Chen, and C. W. Tang. "Organic electroluminescent devices with improved stability." Applied physics letters 69.15 (1996): 2160-2162.

[47] Jeon, Nam Joong, et al. "Solvent engineering for high-performance inorganic–organic hybrid perovskite solar cells." Nature materials (2014).

[48] Kang, Man Gu, et al. "Dependence of TiO~ 2 Film Thickness on Photocurrent-Voltage Characteristics of Dye-Sensitized Solar Cells." BULLETIN-KOREAN CHEMICAL SOCIETY 25.5 (2004): 742-744.

[49] Guo, Xiao-Zhi, et al. "Study on the effect of measuring methods on incident photon-to-electron conversion efficiency of dye-sensitized solar cells by home-made setup." Review of scientific instruments 81.10 (2010): 103106.

[50] Zaban, Arie, Miri Greenshtein, and Juan Bisquert. "Determination of the Electron Lifetime in Nanocrystalline Dye Solar Cells by Open-Circuit Voltage Decay Measurements." ChemPhysChem 4.8 (2003): 859-864.

[51] Nakade, Shogo, et al. "Stepped light-induced transient measurements of photocurrent and voltage in dye-sensitized solar cells: application for highly viscous electrolyte systems." Langmuir 21.23 (2005): 10803-10807.

[52] Yang, Mengjin, et al. "Carrier transport in dye-sensitized solar cells using single crystalline TiO2 nanorods grown by a microwave-assisted hydrothermal reaction." The Journal of Physical Chemistry C 115.30 (2011): 14534-14541.

[53] Xue, Guogang, et al. "Understanding of the chopping frequency effect on IPCE measurements for dye-sensitized solar cells: from the viewpoint of electron transport and extinction spectrum." Journal of Physics D: Applied Physics 45.42 (2012): 425104.

[54] Zhao, Chen, et al. "Revealing Underlying Processes Involved in Light Soaking Effects and Hysteresis Phenomena in Perovskite Solar Cells." Advanced Energy Materials (2015).

[55] https://en.wikibooks.org/wiki/Analogue_Electronics/pn_Junctions

[56] Kim, Hui-Seon, and Nam-Gyu Park. "Parameters affecting I–V hysteresis of CH3NH3PbI3 perovskite solar cells: effects of perovskite crystal size and mesoporous TiO2 layer." The Journal of Physical Chemistry Letters 5.16 (2014): 2927-2934.

[57] Snaith, Henry J., et al. "Anomalous hysteresis in perovskite solar cells." The Journal of Physical Chemistry Letters 5.9 (2014): 1511-1515.